Received: 30 January 2023 | Revised: 1 September 2023 | Accepted: 17 October 2023

DOI: 10.1002/cne.25554

JCN RESEARCH IN SYSTEMS NEUROSCIENCE THE JOURNAL OF COMPARATIVE NEUROLOGY WILEY

RESEARCH ARTICLE

Comparative neuroanatomy of the central nervous system in web-building and cursorial hunting spiders

Philip O. M. Steinhoff[1] | **Steffen Harzsch**[2] | **Gabriele Uhl**[1]

[1]Zoological Institute and Museum, General and Systematic Zoology, University of Greifswald, Greifswald, Germany

[2]Zoological Institute and Museum, Cytology and Evolutionary Biology, University of Greifswald, Greifswald, Germany

Correspondence
Philip O. M. Steinhoff and Gabriele Uhl, Zoological Institute and Museum, General and Systematic Zoology, University of Greifswald, Loitzer Straße 26, 17489 Greifswald, Germany.
Email: philipsteinhoff@gmail.com; gabriele.uhl@uni-greifswald.de

Dedication: We dedicate this article to Friedrich G. Barth, in recognition of his groundbreaking work on spider sensory ecology and neurobiology that will remain the backbone of spider neurobiology research for decades to come.

Funding information
Universität Greifswald, Grant/Award Number: Bogislaw Scholarship; Laudier Histology Cooperation and Travel Grant; Deutsche Forschungsgemeinschaft, Grant/Award Numbers: INST 292/119-1 FUGG, INST 292/120-1 FUGG, UH 87/11-1

Abstract

Spiders (Araneae) include cursorial species that stalk their prey and more stationary species that use webs for prey capture. While many cursorial hunting spiders rely on visual cues, web-building spiders use vibratory cues (mechanosensation) for prey capture. We predicted that the differences in primary sensory input between the species are mirrored by differences in the morphology/architecture of the central nervous system (CNS). Here, we investigated the CNS anatomy of four spider species, two cursorial hunters *Pardosa amentata* (Lycosidae) and *Marpissa muscosa* (Salticidae), and two web-building hunters *Argiope bruennichi* (Araneidae) and *Parasteatoda tepidariorum* (Theridiidae). Their CNS was analyzed using Bodian silver impregnations, immunohistochemistry, and microCT analysis. We found that there are major differences between species in the secondary eye pathway of the brain that pertain to first-order, second-order, and higher order brain centers (mushroom bodies [MB]). While *P. amentata* and *M. muscosa* have prominent visual neuropils and MB, these are much reduced in the two web-building species. *Argiope bruennichi* lacks second-order visual neuropils but has specialized photoreceptors that project into two distinct visual neuropils, and *P. tepidariorum* lacks MB, suggesting that motion vision might be absent in this species. Interestingly, the differences in the ventral nerve cord are much less pronounced, but the web-building spiders have proportionally larger leg neuropils than the cursorial spiders. Our findings suggest that the importance of visual information is much reduced in web-building spiders, compared to cursorial spiders, while processing of mechanosensory information requires the same major circuits in both web-building and cursorial hunting spiders.

KEYWORDS
Arachnida, Bodian staining, lifestyle, neuroanatomy, sensory ecology, visual neuropils, volumes

1 | INTRODUCTION

Differences in the specific lifestyle of closely related animal species are mirrored in the relative size and wiring of different central nervous system (CNS) areas. This is particularly evident when lifestyles rely on specific sensory modalities, such as vision in whirligig beetles (Strausfeld et al., 2009), visual and olfactory cues in butterflies that use different food sources (Couto et al., 2020; Montgomery et al., 2021), or differences in feeding ecology in primates (Louail et al., 2019). Spiders (Araneae) represent a group of predators that have evolved a wide range of lifestyles, particularly with regard to foraging strategies that depend strongly on vision or vibration (Foelix, 2011). We can expect that such lifestyle-specific sensory input is reflected in the structure of the CNS (cf. Chittka & Niven, 2009). However, while sensory systems in spiders have been well studied (reviewed in Barth, 2002), our knowledge of spider CNS anatomy is mainly derived from one species with a cursorial lifestyle, the wandering spider *Cupiennius salei* (Keyserling, 1877) (Anton & Tichy, 1994; Babu & Barth, 1984, 1989; Loesel et al., 2011; Schmid & Becherer, 1999; Schmid & Duncker, 1993; Strausfeld & Barth, 1993; Strausfeld et al., 1993). Studies on the brains of other spider species have specifically focused on details of the visual system (Hanström, 1921; Kovoor et al., 2005; Long, 2021; Steinhoff et al., 2020).

The CNS of spider species studied so far is composed of highly fused ganglia: the ventral nerve cord (VNC), which consists of the posterior opisthosomal neuropil (OpN), four paired leg neuropils (LNs 1–4) and a central area with different neuropilar structures that receive primary sensory input from sensilla located on the legs and pedipalps (Anton & Tichy, 1994; Babu & Barth, 1984, 1989). The brain, which is located anterio-dorsal of, and fused with the VNC, is composed of the three neuromeres trito-, deuto-, and protocerebrum (Lehmann et al., 2016; Scholtz & Edgecombe, 2006; Steinhoff et al., 2017). A distinct border between the different neuromeres is usually not discernable, and the tripartition of the brain has been subject to a long-lasting debate. While the deutocerebrum was considered absent in chelicerates by several authors (Babu, 1965; Bitsch & Bitsch, 2007; Wegerhoff & Breidbach, 1995; Weygoldt, 1975, 1985), more recent molecular and embryological studies concluded that the segmentation of the chelicerate brain is tripartite (Brenneis et al., 2008; Damen & Tautz, 1998; Mittmann & Scholtz, 2003; Scholtz & Edgecombe, 2006; reviewed in Scholtz, 2016). The tritocerebrum is largely made up of the pedipalpal neuropil (PdN) and situated just below (ventral of) the esophagus, while the deutocerebrum contains the cheliceral neuropil (ChN) and is situated lateral and dorsal of the esophagus (Babu & Barth, 1984; Lehmann et al., 2016; Steinhoff et al., 2017). The protocerebrum is the dorsalmost neuromere of the brain and is composed of a central neuropilar area (protocerebral neuropil, PN), the higher order integration neuropils arcuate body (AB), and mushroom bodies (MB), as well as the visual neuropils (Babu & Barth, 1984; Steinhoff et al., 2020).

Most spiders possess four pairs of eyes, one of which distinctively differs from the others in anatomy and development (Land, 1985; Morehouse et al., 2017). The principal eyes (or anterior median eyes, AME) have a movable retina, are able to detect colors, and are used for object recognition (Barth et al., 1993; Land, 1985; Schmid, 1998; Yamashita & Tateda, 1976, 1978). The secondary eyes (comprising anterior lateral eyes [ALE], posterior lateral eyes [PLE], and posterior median eyes [PME]), differ considerably between spider families (Homann, 1950, 1952) but have retinae that are not movable, cannot distinguish colors, and are used for motion detection (Land, 1985; Morehouse et al., 2017; Schmid, 1998). The principal eye pathway in the brain is similar in all spider species investigated so far and consists of a first-order (AM1), second-order (AM2), and higher order (AB) neuropil (Steinhoff et al., 2020; Strausfeld et al., 1993). The secondary eye pathway shows pronounced variation between different spider species (Hanström, 1921; Long, 2021; Steinhoff et al., 2020). While in *C. salei*, every secondary eye serves its own first- and second-order visual neuropils (Babu & Barth, 1984; Strausfeld & Barth, 1993), this is not the case in jumping spiders, in which two shared second-order visual neuropils exist, and the PME is only connected to a single visual neuropil (Steinhoff et al., 2020). Hanström (1921) compared the visual systems of the secondary eyes of three families of web-building spiders with two families of cursorial hunting spiders. He found only a single visual neuropil for all secondary eyes in the web-building spiders, in contrast to large first- and second-order visual neuropils in wolf spiders and jumping spiders (Hanström, 1921). Long (2021) investigated the secondary eye visual neuropils of species from 19 different families across the spider tree of life and categorized them based on the presence and size of the neuropils into four groups: (1) spiders with a single visual neuropil; (2) spiders with a single visual neuropil and MB; (3) spiders with a first-order visual neuropil, a small second-order visual neuropil, and MB; and (4) spiders with large first- and second-order visual neuropils and large MB. Perhaps not surprisingly, these differences in neuropil number in the secondary eye visual pathway also result in volumetric differences in visual and higher-order neuropils of different spider species as shown by Weltzien and Barth (1991) and Long (2021).

To date, it remains unclear whether the differences in spider brain anatomy are restricted to visual brain areas. This study therefore investigates, whether other regions of the CNS show similar differences that can be related to the sensory ecology of the species studied. We compare two cursorial spider species that roam freely and attack prey when encountering it and two web-building spiders that are relatively stationary and catch prey with their web in which they also reproduce. Among the cursorial hunters, we selected the salticid *Marpissa muscosa* (Clerck, 1757) and the lycosid *Pardosa amentata* (Clerck, 1757); among the web-building spiders, we chose the araneid *Argiope bruennichi* (Scopoli, 1772) and the theridiid *Parasteatoda tepidariorum* (C. L. Koch, 1841). These species have been studied in terms of their ecology, mating behavior, and developmental biology (see below); thus, our study contributes to a considerable body of knowledge. We compare our findings on the anatomy of the CNS in these species with that of the well-studied ctenid spider *C. salei* (Babu & Barth, 1984, 1989; Strausfeld & Barth, 1993; Strausfeld et al., 1993) and discuss what we can learn from our findings about the sensory ecology of spiders.

2 | MATERIAL AND METHODS

2.1 | Experimental animals

Adult females of the following species: *A. bruennichi*, *M. muscosa*, and *P. amentata*, were collected in and near Greifswald (Germany) and processed for histology and microCT immediately. Individuals of the species *P. tepidariorum* were collected in the greenhouses of the botanical garden of the University Greifswald and reared in climate chambers (26°C, 80% humidity, 12/12 h light cycle). *Parasteatoda tepidariorum* individuals were kept individually in plastic boxes of 145 × 110 × 68 mm size that were enriched with paper tissue.

2.2 | MicroCT analysis and volume calculation

Prosomata were fixed in fresh acetic alcohol formalin solution (AAF; 10 mL 16% paraformaldehyde, 2.5 mL glacial acetic acid, 42 mL 80% ethanol) at room temperature for 4 h. Samples were dehydrated in a graded ethanol series (70%, 80%, 90%, 96%, and 3 × 99.8% ethanol for 30 min each) and then transferred to a 1% iodine solution (iodine, resublimated [Carl Roth, X864.1] in 99.8% ethanol) for 48 h to enhance tissue contrast. Samples were subsequently washed three times in 99.8% ethanol, mounted in fresh 99.8% ethanol, and scanned once (overview scan of the entire prosoma; Sombke et al., 2015). Afterward, samples were critical point dried with an automated dryer (Leica EM CPD300) using slow CO_2 admittance with a delay of 120 s, 30 exchange cycles (CO_2 : 99.8% ethanol), followed by a slow heating process and slow gas discharge. Dried prosomata were mounted using a conventional glue gun onto plastic rods so that the AME were oriented upward.

MicroCT scans were carried out with an optical laboratory-scale X-ray microscope (Zeiss XradiaXCT-200; Sombke et al., 2015). Scans were performed with a 4x or a 10x objective lens unit using the following settings: 40 kV, 8 W, 200 μA, and exposure times between 0.5 and 3s. Scans took between 1 and 2 h and resulted in pixel sizes between 1.7 and 5.5 μm. Reconstruction of tomographic projections was done using the XMReconstructor software (Zeiss), resulting in image stacks (TIFF format). All scans were performed using Binning 2 for noise reduction (summarizing 4 pixels) and were reconstructed with full resolution (using Binning 1).

The volumes of the different neuropilar structures were calculated using AMIRA 5.4.5 and 6.0.0 (Visualization Science Group, FEI). Since we were comparing different species with different body sizes, it was necessary to calculate the amount of shrinkage of the tissue for each specimen (Rivera Quiroz & Miller, 2022). To do this, the CNS volume in both the wet and the dried condition and the factor by which the two differed was calculated. This factor was later used to adjust the volumes of the different brain regions, which were reconstructed and calculated from the dried scans. In order to account for individual variation, we reconstructed the CNS structures of three specimens per species and used the mean for comparison (given in percentage of total CNS neuropil volume). A full table of all calculated volumes is available from Morphobank (see Data Availability Statement).

2.3 | Azan staining

The prosomata of two females of each species were fixed in Gregory's artificially aged Bouin solution (Gregory, 1980). After 4 days in fixative, the prosomata were dehydrated through a graded ethanol series (80%, 90%, and 3 × 96% ethanol for 20-min each) and were then transferred for 2 h into a 1:1 solution of 96% ethanol:tetrahydrofuran (Carl Roth, CP82.1) at room temperature. Samples were kept for 24 h in pure tetrahydrofuran followed by 24 h in a solution of 1:1 tetrahydrofuran and paraffin (Carl Roth, 6643.1) at 60°C. Afterward, samples were transferred to 100% paraffin at 60°C for 48 h and then embedded in fresh paraffin. Sagittal sections (5 μm) were cut with a motorized rotary microtome (Microm HM 360). Sections were stained with Azan according to Geidies (Schulze & Graupner, 1960) and mounted in Roti-Histokitt II (Carl Roth, T160.1).

2.4 | Bodian reduced silver staining

Following anesthetization with CO_2 and removal of the opisthosoma and legs (without coxae), the prosomata of several individuals of the four focal species were fixed in AAF solution (42 mL 80% ethanol, 10 mL16% paraformaldehyde (PFA), 2.5 mL acetic acid). After 4 h in fixative, the prosoma was dehydrated through a graded ethanol series (70%, 80%, 90%, 96%) and was then transferred for 2 h into a 1:1 solution of 96% ethanol:tetrahydrofuran (Carl Roth, CP82.1). Samples were kept for 24 h in 100% tetrahydrofuran followed by 24 h in a solution of 1:1 tetrahydrofuran and paraffin (Carl Roth, 6643.1). Afterwards, samples were embedded in pure paraffin. Horizontal, frontal, and sagittal sections (15 μm) were made with a motorized rotary microtome (Microm HM 360) and subsequently stained according to the original Bodian method (Bodian, 1936). Sections were rehydrated through an ethanol series (Roti Histokit, terpineol, 100%, 90%, 70%, 50% ethanol) and incubated overnight at 60°C in a 2% protargol solution. Protargol was synthesized according to the recipe by Pan et al. (2013). To achieve an ideal staining result, the pH was set to 8.0. No copper was added to the solution, as we found that even a small amount (0.25%) increased the selectivity of the stain to an undesired degree. In the morning, the staining jar was allowed to cool to room temperature, and sections were briefly rinsed in double distilled water (ddH_2O) and then developed in a 1% hydroquinone/ 2% sodium sulfite mixture in ddH_2O for 5 min. Afterward, sections were rinsed under running tap water for 3 min and then placed in a solution of 1% gold chloride in ddH_2O for 10 min. Sections were then rinsed in two changes of ddH_2O for 15 s each and placed in a 4% oxalic acid solution for 8 min. Following two additional rinses in ddH20 for 15 s each, sections were placed in 10% sodium thiosulfate for 5 min. Finally, sections were

TABLE 1 Primary and secondary antibodies.

Labeling reagent	Dilution and specifications
Primary	
Monoclonal anti-synapsin antibody produced in mouse (RRID AB_528479)	1:1000, DSHB 3C11; Steinhoff et al. (2017, 2020), this study
Polyclonal anti-acetylated α-tubulin antibody produced in rabbit (RRID AB_2637882)	1:1000, 1:250, ThermoFisher PA5-58711
Secondary	
Polyclonal Cy3 anti-mouse IgG secondary anti- body produced in goat (RRID AB_2338680)	1:500, Jackson Immuno Research, 115—165-003
Polyclonal Alexa 488 anti-rabbit IgG secondary antibody produced in goat (RRID AB_2534074)	1:500, Invitrogen, A11006
Hoechst 33258	1:1000, Sigma 14530

TABLE 2 Methods and antisera combinations.

Methods	Antisera combinations/staining	Combined with	Specimens
Wholemount	Anti-synapsin (mouse)	Cy3 anti-mouse (goat)	2
	Anti-acetylated-α-tubulin (rabbit)	Alexa Fluor 488 anti-rabbit (goat)	
Vibratome sections (60 & 80 μm)	Anti-synapsin (mouse)	Cy3 anti-mouse (goat)	12
	Anti-acetylated-α-tubulin (rabbit)	Alexa Fluor 488 anti-rabbit (goat) Nuclear labeling: Hoechst 33258	
Wholemount	Micro-emerald dye	/	5
	anti-synapsin (mouse)	Cy3 anti-mouse (goat)	
Paraffin sections (15 μm)	Bodian silver impregnation	/	20
microCT scans	1% idodine (in 99% ethanol)	/	12

washed two times in ddH20 for 8 min, dehydrated through an ethanol series (the inverse of the series above) and mounted in Roti-Histokitt II (Carl Roth, T160.1) under glass slides. The protocol described above consistently yielded very good staining of *P. amentata*, *M. muscosa*, and *P. tepidariorum* sections. However, no consistent results were obtained for *A. bruennichi*, as often only a few neurites were recognizable. In some series, individual sections stained well, while in other series, only parts of sections or none at all showed the desired degree of selectivity. We tried variations of the above Bodian staining protocols following the recommendations of Gregory (1980) but none of them produced satisfactory results in *A. bruennichi*. Interestingly, staining attempts in related species (*A. lobata*, *Araneus cornutus*) did not work either, possibly due to specific tissue properties in orb weavers.

2.5 | Anterograde tracing of retinula cells

To clarify the identity of the visual neuropils, the axons of retinula cells (RCA) of the different secondary eyes were traced in *A. bruennichi* and *P. tepidariorum*. The spiders were anesthetized with CO_2 and immobilized on a dissection dish filled with plasticine, using insect pins and a piece of fine mesh. A tiny hole was pierced into one of the eyes using a custom-made manual micromanipulator and a minutia. Using thin forceps, a crystal of micro-emerald (dextran fluorescein with biotin, 3000 MW, D7156; ThermoFisher) was inserted through the hole in the eye. The hole was then sealed with Vaseline. The preparations were stored overnight at 4°C so that the dye had sufficient time to reach the termination sites of the RCA. The next morning, the spiders were dissected, and the CNS with eye nerve and retinae attached was isolated and fixed overnight in 2% PFA. After several washing steps in PBS, the brains were immunostained with anti-synapsin (see details below; Tables 1 and 2). Finally, the tissue was cleared in RapiClear (SunJin Lab) and imaged with a Leica SP5 II confocal microscope.

2.6 | Immunohistochemistry

Three different combinations of markers were used to visualize neuropils and connecting neurites in the CNS of the four focal spider species (see Table 1 for a list of marker combinations used and Table 2 for specifications of labeling reagents).

Individuals of the four species (details Table 2) were anesthetized with CO_2, and then their brains were dissected in PBS and fixed overnight at 4°C in 2% PFA. The brains were washed six times in PBS for 15 min each and then immersed in Poly-L-Lysin (Sigma-Aldrich, P4707) for 1 min. Samples were then embedded in 4% agarose (Sigma-Aldrich, A9414) and sectioned (50 or 80 μm) using a Microm HM 650 V vibratome. After permeabilization in PBS-TX (PBS; 0.3% Triton X-100 [Sigma-Aldrich, X100]; 1% bovine serum albumin [Sigma-Aldrich, A2153]; 0.05% Na-acide; or alternatively PBS; 0.5% Triton;

1.5% dimethylsulfoxide [DMSO]) for 1 h at room temperature, incubation in primary antibodies was performed overnight at 4°C or room temperature. The sections were washed several times with PBS-TX after incubation. Incubation in secondary antibodies or counterstains was done overnight at 4°C or room temperature. After repeated washing in PBS, the sections were mounted in Mowiol (Merck 475904).

Two individuals of *P. tepidariorum* were processed as whole-mounts, according to an adapted protocol after Ott (2008; see also Steinhoff et al., 2017). Brains were dissected in TRIS buffer (0.1 M, pH 7.4 [Carl Roth, 4855]), and fixed in zincformaldehyde at room temperature with gentle shaking for several days. The brains were then washed three times for 15 min each in TRIS buffer and incubated for 2 h in a 4:1 mixture of methanol and DMSO (Carl Roth, 4720). After incubation in 100% methanol for 1 h, the brains were rehydrated in a graded series of methanol (90%, 70%, 50%, and 30%) for 10 min each and washed in TRIS buffer. The brains were then permeabilized in PBS-DMSO (PBS, 5% bovine serum albumin, 1% DMSO, 0.05% Na-acide) for 2 h at room temperature and incubated in the primary antibody at 4°C for 4 days. The brains were then washed several times in PBS-DMSO for 2 h and incubated in secondary antibody for 4 days at 4°C. They were then transferred to a graded glycerol series containing 1%, 2%, and 4% (each for 2 h) and 8%, 15%, 30%, 50%, 60%, 70%, and 80% (each for 1 h) glycerol in TRIS buffer and 1% DMSO. After five changes in pure ethanol for 30 min each, the brains were mounted in fresh methyl salicylate (Sigma, 76631). We replaced the primary antibodies with PBS-TX in control experiments and did not detect any neuronal labeling.

2.7 | Microscopy, image processing, and nomenclature

Immunohistochemically labeled sections and wholemounts were examined with a Nikon eclipse 90i microscope and imaged with a Leica SP5 II confocal microscope (cLSM). Serial Bodian-stained paraffin sections were examined and photographed with a Nikon eclipse 90i microscope at 20x magnification. Alignment of images from Bodian-stained sections was carried out using the TrakEM2 module in ImageJ 1.52i and the AlignSlices module in AMIRA 5.4.5. Three-dimensional visualizations of Bodian and microCT image stacks were performed using AMIRA 5.4.5 and 6.0.0 (Visualization Science Group, FEI). Drawings and figure plates were created using Corel PaintShop Pro 21.0 and CorelDRAW 20.1. The images were processed in Corel Paint Shop Pro with global contrast and brightness adjustment functions. The terminology used for CNS structures is consistent with Richter et al. (2010). For spider-specific CNS structures, we follow the terminology of Steinhoff et al. (2020), Strausfeld et al. (1993), Strausfeld and Barth (1993), and (specifically with regard to tracts in the VNC) Babu and Barth (1984, 1989). We have changed some of the original abbreviations introduced by Babu and Barth (1984, 1989) but give the original abbreviation in brackets behind the abbreviation used here. Positional data are given in relation to the body axis. We refer to results from immunohistochemical experiments as immunoreactivity, for example, synapsin immunoreactivity.

List of abbreviations used in the text with previous abbreviations used by other authors for the same structures, if applicable.

Abbreviations	Abbreviations as used by Babu and Barth (1984)	Structure
AB	CB	Arcuate body
ABd		Arcuate body, dorsal lobe
ABv		Arcuate body, ventral lobe
ALE	ALE	Anterior lateral eyes
AL1	ALOL	First-order visual neuropils of ALE
AL2		Second-order visual neuropils of ALE
AME	AME	Anterior median eyes
AM1	AMOL	First-order visual neuropils of AME
AM2	AMOM	Second-order visual neuropils of AME
ASc		Anterior stomodeal commissure
Bc3-5		Brain commissure 3–5
BN		Blumenthal neuropil
BVt	BVT	Brain vertical tract
Cc	CC	Central commissure
Chc		Cheliceral commissure
Chc2		Cheliceral commissure 2
ChN	CHG	Cheliceral neuropil
CLt	CL	Centro-lateral tract
CTt	CT	Central tract
cVNC		Central part of the ventral nerve cord
Dc	DC	Dorsal commissure
Dcb		Deutocerebrum
L2		Additional second order visual neuropil of ALE and PLE in *M. muscosa*
LCt	LCT	Lateral cerebral tract
LN 1–4	AMG 1–4	Leg neuropils 1–4
LSAt	LSAT	Lateral sensory association tract
MB		Mushroom bodies
MBb	BRG	Mushroom body bridge
MBb2		Mushroom body bridge 2
MBd		Mushroom body head
MBh	PD	Mushroom body haft
MBp	HT	Pedunculus of the mushroom body

(Continues)

Abbreviations	Abbreviations as used by Babu and Barth (1984)	Structure
MCt	MC	Mid-central tract
MCc	MCC	Mid-central commissure
MDc	MDC	Mid-dorsal commissure
MeCt	MCT	Median-cerebral tract
MDt	MD	Mid-dorsal tract
MDc	MDC	Mid-dorsal commissure
MVt	MV	Mid-ventral tract
OE	OES	Esophagus
OpN	OPiG	Opisthosomal neuropil
PCc	PCC	Protocerebral commissure
PCDt	PCDT	Protocerebro-dorsal tract
PCMt	PCMT	Protocerebro-median tract
PCVt	PCVT	Protocerebro-ventral tract
PdN	PDG	Pedipalpal neuropil
Pdp		Pedipalpal projection
Pdc		Pedipalpal commissure
Pdc2		Pedipalpal commissure 2
PLE	PLE	Posterior lateral eyes
PL1	PLOL	First-order visual neuropils of the PLE
PL2		Second-order visual neuropils of the PLE
PME	PME	Posterior median eyes
PM1	PMOL	First-order visual neuropils of the PME
PM2		Second order visual neuropils of the PME
PN		Protocerebral neuropil
PrincVis		Combined first- and second-order visual neuropils of the principal eyes
PSc		Posterior stomodeal commissure
RCA		retinula cell axons
SC		Soma cortex
SecVN1		First-order visual neuropils of all secondary eyes (ALE, PLE, PME)
SecVN2	OMSE	Second-order visual neuropils of all secondary eyes (ALE, PLE, PME)
SecVis		Combined first- and second-order visual neuropil(s) of the secondary eyes
SLt	SLT	Sensory longitudinal tract
ST		Sucking stomach
STb		Stomodeal bridge
Tcb		Tritocerebrum
Vc	VC	Ventral commissure
VisN		Visual neuropils
VLt	VL	Ventro-lateral tract
VMt	VMT	Ventral median tract
VNC		Ventral nerve cord

(Continues)

3 | RESULTS

3.1 | General organization of the CNS

The CNS comprises the dorsal brain and a fused VNC. The brain is composed of three neuromeres, the trito-, deuto-, and protocerebrum. The tritocerebrum is situated below the esophagus and formed by the PdN, while the deutocerebrum borders the esophagus laterally, extends slightly above it (dorsal of it) and consists of the ChN. The protocerebrum is the dorsalmost neuromere of the brain and consists of a central neuropil with many tracts, the AB, and visual neuropils. We describe the CNS of the four focal spider species (Figure 1) from dorsal to ventral, starting with the visual system (Figures 2–6), followed by higher order neuropils and tracts in the protocerebrum (Figures 7–9), the deuto- and tritocerebrum (Figure 10), and the VNC (Figures 11–14). The VNC consists of a central neuropil rich in tracts (central VNC [cVNC], see details below), four paired LNs and a posterior OpN. The entire CNS is surrounded by a soma cortex, which is thickest ventral of the VNC, whereas only a thin layer of very few somata is observed dorsal of the VNC (Figure 14a). We could distinguish two cell types: giant somata, which are found in small numbers and only ventral of the VNC (Figures 8d and 14a) and regular somata that are most densely packed anterior of the PN (e.g., Figure 2a,d). For every aspect, we describe *P. amentata* first because its CNS is most similar to that of *C. salei*, and then highlight the differences in the other three species, *M. muscosa*, *A. bruennichi*, and *P. tepidariorum*. We briefly describe the visual system in *M. muscosa*, as we explored it in detail in a previous study (Steinhoff et al., 2020). Three-dimensional PDFs with all reconstructed neuropils and tracts for all species are available at Morphobank (see Data Availability Statement).

3.2 | Principal eye pathway

In *P. amentata*, the retina of the principal eyes is connected to its first-order neuropil (AM1) by long RCA (Figure 5a). The AM1 is cup-shaped

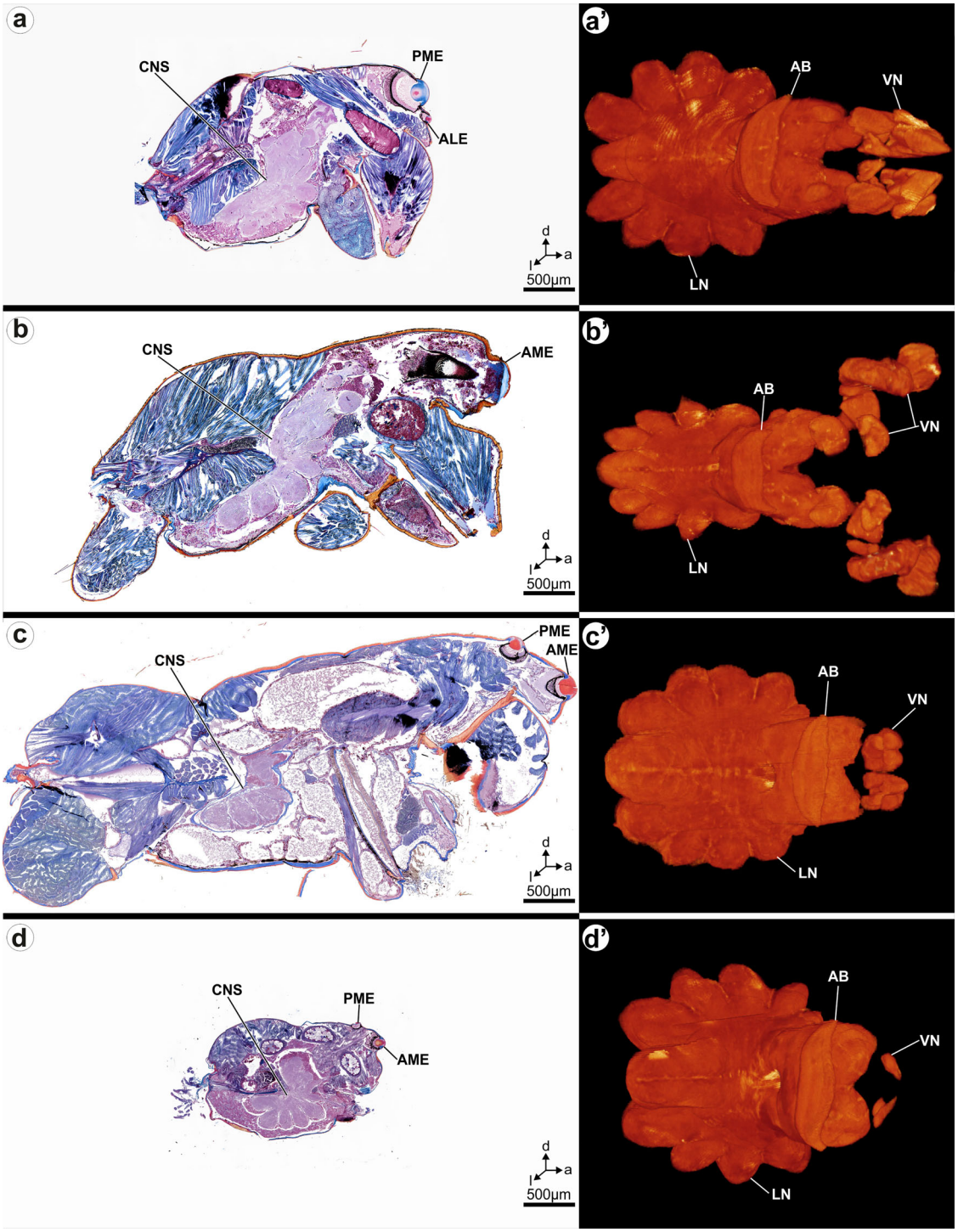

FIGURE 1 Azan-stained mid-sagittal sections of prosomata (a, b, c, d) and 3D reconstructions of the CNS of all focal species (a', b', c', d'). (a, a') *Pardosa amentata*, (b, b') *Marpissa muscosa*, (c, c') *Argiope bruennichi*, and (d, d') *Parasteatoda tepidariorum*. AB, arcuate body; AME, anterior median eye; ALE, anterior lateral eye; CNS, central nervous system; LNs, leg neuropils; PME, posterior median eye; VNs, visual neuropils. (b) adapted from Steinhoff et al. (2017).

(Figure 2b-b') and situated posterior to the first-order visual neuropils of the secondary eyes (see section below), embedded in the anterior soma cortex. It is connected to the second-order visual neuropil (AM2) by a neurite bundle (Figure 2b-b'). The AM2 is of oval shape, and a neurite tract projects from it into the posterior brain region and connects to the AB (Figure 2b-b'). This general arrangement is the same in all four species studied, although in *M. muscosa*, the AM1 is clearly subdivided into distinct regions (Figure 2a; cf. Steinhoff et al., 2020). The AM1 in *A. bruennichi* is the dorsalmost neuropil and is situated anteriorly of the dorsal soma cortex (Figure 2c-c'). The AM2 is located at

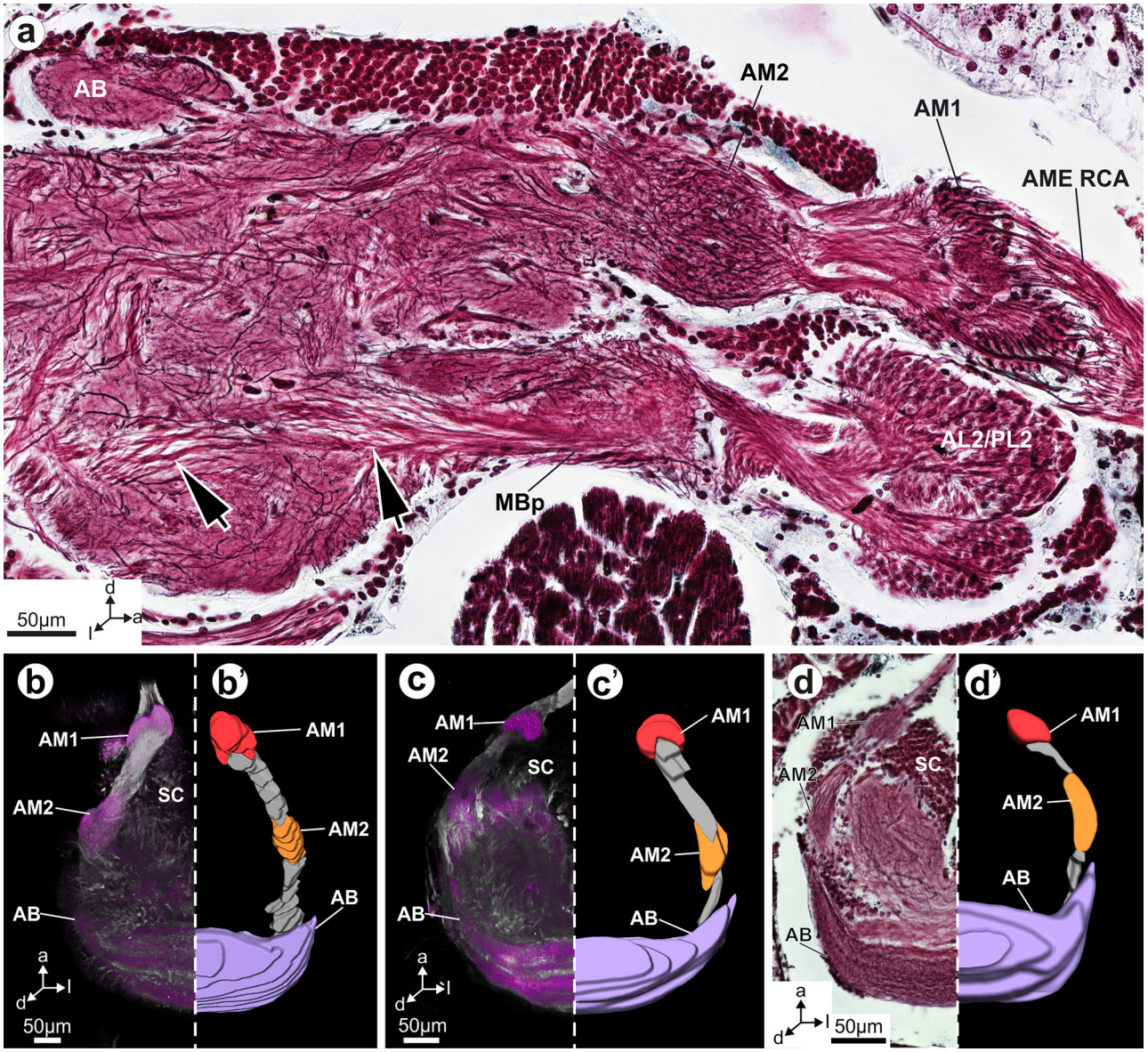

FIGURE 2 The principal eye pathway. (a) Sagittal Bodian-stained section of the protocerebrum in *M. muscosa* showing neurites connecting the AM1 with the AM2, as well as a chiasm of neurites connecting the AL2/PL2 to the MBp. Arrowheads point to neurites connecting the MB with the VNC. (b, c) Maximum projections of image stacks (cLSM) showing synapsin immunoreactivity (magenta) and tubulin-immunoreactivity (gray). (b) In *P. amentata* the AM1 is connected to the AM2 via tightly adjoining neurites, other neurites project from the AM2 to the AB. (b', c', d') Three-dimensional reconstructions based on serial Bodian-stained sections. (b') Visual pathway of the principle eyes in *P. amentata*. (c) In *A. bruennichi*, the AM1 is connected to the AM2, while the AM2 sends neurites toward the outer tips of the AB. (c') Visual pathway of the principle eyes in *A. bruennichi*. (d) In *P. tepidariorum*, Bodian-stained sections reveal thin neurites connecting the AM1 with the AM2 and the latter with the AB. (d') Visual pathway of the principle eyes in *P. tepidariorum*. a, anterior; AL2/PL2, second-order visual neuropil of anterior lateral and posterior lateral eyes; AB, arcuate body; AME RCA, retinula cell axons of the anterior median eyes; AM1, first-order visual neuropil of the anterior median eyes; AM2, second-order visual neuropil of the anterior median eyes; d, dorsal; l, lateral; MBp, mushroom body pedunculus; SC, soma cortex.

the outer rim of the brain, has weak synapsin immunoreactivity, and its shape is less well distinguishable from the surrounding neuropil than in *P. amentata* (Figure 2c). In *P. tepidariorum*, the AM1 is roundish instead of cup-shaped and situated more anterior than in *P. amentata* (Figure 2d-d'). The AM2 has a slender oval shape and is less clearly distinguishable from the surrounding PN (Figure 2d).

3.3 | Secondary eye pathway

In *P. amentata*, each eye supplies its own first-order visual neuropil via long RCA that extends in a single bundle through the anterior prosoma along with the nerve of the principal eyes (Figure 5a). The first-order visual neuropil of the PME (PM1) is the largest and most dorsally

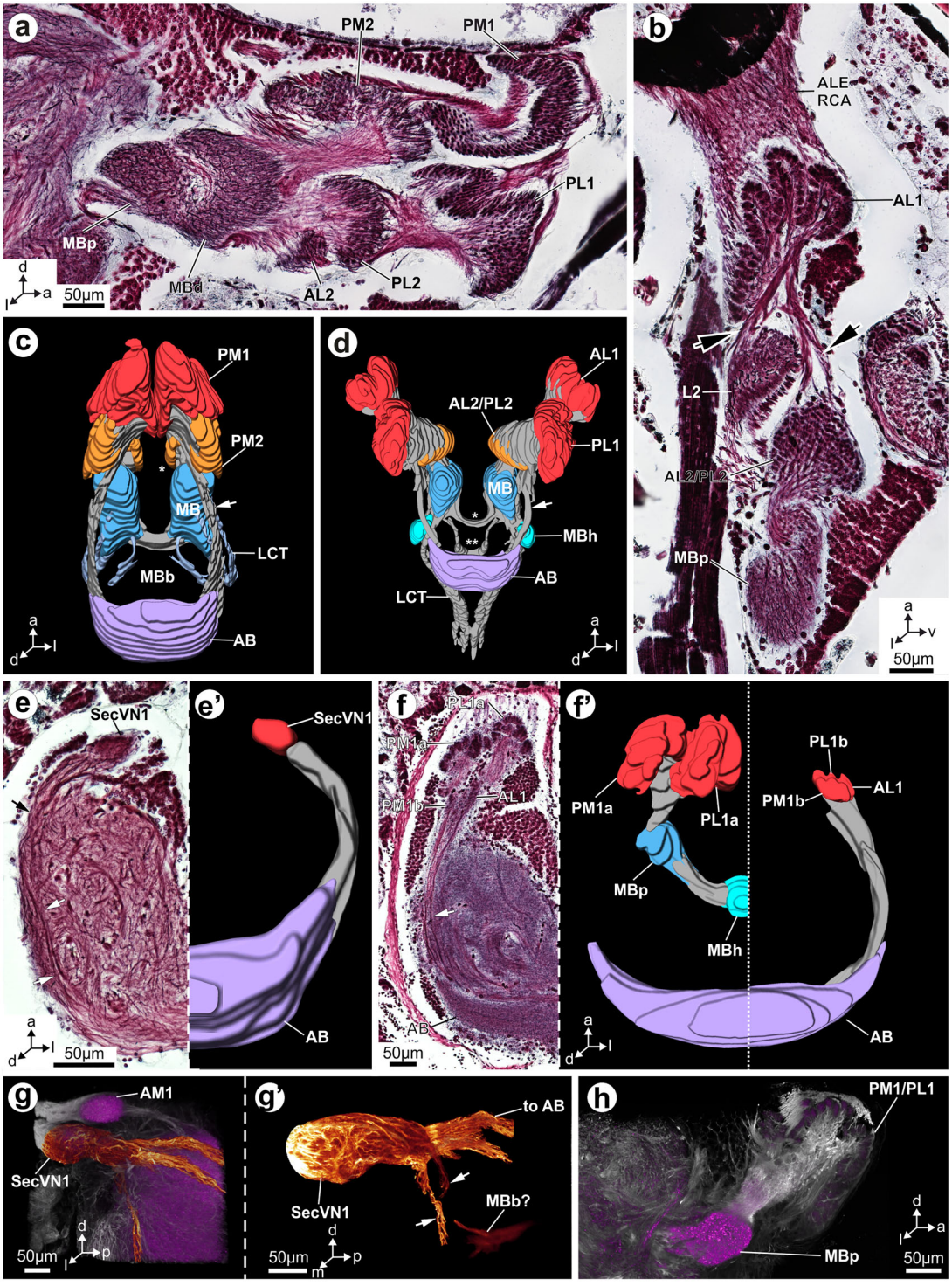

FIGURE 3 The secondary eye pathway. (a, b, e, f) Bodian-stained sections. (c, d, e', f') Three-dimensional reconstructions based on serial Bodian-stained sections. (g-h) Maximum projections of image stacks (cLSM) showing synapsin immunoreactivity (magenta) and tubulin-immunoreactivity (gray and gold). (a) Sagittal section showing the secondary eye visual system of *P. amentata*. Every eye serves its own first- and second-order neuropil and the second-order neuropils connect to the MBd. The MBd is closely connected to the MBp. (b) Sagittal section showing the secondary eye visual system of *M. muscosa*. The ALE (and PLE, not shown) connect to their own first-, but two shared second-order visual neuropils. Arrows show connections between AL1 and L2 and between AL1 and AL2/PL2. AL2/PL2 further connects to the MBp. (c) Three-dimensional reconstruction of the secondary eye visual system of *P. amentata*. All first-order visual neuropils of the secondary eyes (PL1 and AL1 obscured by PM1, which is most dorsal), connect to their second-order neuropils and directly to the AB. * shows the AL2. The LCt connects the MB to the VNC. (d) Three-dimensional reconstruction of the secondary eye visual system of *M. muscosa*. * shows the MBb, ** the MBb2. Arrow points to direct connection between first-order visual neuropils and the AB. The LCt connects the MB to the VNC. (e) Horizontal section showing

(Continues)

FIGURE 3 (Continued)
the secondary eye visual system of *P. tepidariorum*. Arrows point to neurites connecting the SecVN1 with the AB. (e') Three-dimensional reconstruction of the secondary eye visual system of *P. tepidariorum*. (f) Horizontal section showing the secondary eye visual system of *A. bruennichi*. Arrowhead points to neurites connecting PM1b, PL1b, and AL1 with the AB. (f') Three-dimensional reconstruction of the secondary eye visual system of *A. bruennichi*, left half shows connections of PM1a and PL1a to the MBp, right half shows connections of PM1b, PL1b, and AL1 to the AB. The MBh is located medially. (g) Secondary eye visual neuropil and tracts in *P. tepidariorum*. SecVN1 is located just ventral of the AM1, bundles of neurites connecting it to other brain regions are highlighted. (g') Isolated visual tracts and potential MBb in *P. tepidariorum*. (h) PM1 and PL1 connect directly to the MBp in *A. bruennichi*. a, anterior; AB, arcuate body; ALE RCA, retinula cell axons of the anterior lateral eyes; AL1, first-order visual neuropil of the anterior lateral eyes; AL2, second-order visual neuropil of the anterior lateral eyes; AL2/PL2, second-order visual neuropil of anterior lateral and posterior lateral eyes; AM1, first-order visual neuropil of the anterior median eyes; d, dorsal; l, lateral; L2, shared second-order visual neuropil of the anterior lateral and posterior lateral eyes; LCt, lateral cerebral tract; MB, mushroom body; MBb, mushroom body bridge; MBb2, mushroom body bridge 2; MBd, mushroom body head; MBh, mushroom body haft; MBp, mushroom body pedunculus; PL1, first-order visual neuropil of the posterior lateral eyes; PL1a, first-order visual neuropil of the posterior lateral eyes a; PL1b, first-order visual neuropil of the posterior lateral eyes b; PL2, second-order visual neuropil of the posterior lateral eyes; PM1, first-order visual neuropil of the posterior median eyes; PM1a, first-order visual neuropil of the posterior median eyes a; PM1b, first-order visual neuropil of the posterior median eyes b; PM2, second-order visual neuropil of the posterior median eyes; SecVN1, first order visual neuropil of the secondary eyes; v, ventral.

located visual neuropil. The first-order visual neuropil of the PLE (PL1) is only slightly smaller and similarly shaped, lying just below the PM1 (Figures 3a,c and 5a). The first-order visual neuropil of the ALE (AL1) is much smaller than the PM1 and PL1 and nested within the visual neuropils posterior of the ventralmost part of the PL1 (Figures 3a,c and 5a). All first-order visual neuropils send long conspicuous axons along the brain margin into the region immediately anterior and ventral of the AB, where they form an arch and probably terminate (Figures 3c and 5a). In addition, each first-order visual neuropil supplies its own second-order visual neuropil (PM2, PL2, and AL2), which are glomerular in structure and located directly posterior of their first-order visual neuropil (Figures 3a,c and 5a). While PM2 and PL2 are both slightly smaller than PM1 and PL1, respectively, AL2 is similar in size to AL1 (Figures 3a,c and 5a). All three second-order visual neuropils send most of their axons to the anterior part of the MB, the mushroom body head (MBd; Figures 3a,c and 5a). This arrangement found in *P. amentata* contrasts with the situation in *M. muscosa*, where the first-order visual neuropils of the AL1 and PL1 are connected to two second-order visual neuropils (AL2/PL2 and the additional L2), and the small PM1 is only connected to the AB (Figures 3b,d and 5b). While AL1 and PL1 are also connected to the AB, AL2/PL2 and L2 are all connected to the MB in *M. muscosa* (Figures 3b,d and 5b; cf. also Steinhoff et al., 2020).

In *A. bruennichi*, anti-synapsin labeling and Bodian staining show that the RCA of the secondary eyes terminates in two closely adjacent, anterior cauliflower-shaped neuropils and a smaller, tripartite finger-shaped neuropil, which is located just posterior of the cauliflower-shaped neuropils (Figure 4a–c). Dye backfills from the different secondary eyes reveal that the posterior-median eyes send RCA only into the more medial cauliflower-shaped neuropil (PM1a) and the left (closest to the midline of the brain) "finger" of the tripartite neuropil (PM1b; Figure 4a). The RCA of the posterior-lateral eyes, on the other hand, terminate in the more lateral cauliflower-shaped neuropil (PL1a) and the medial "finger" of the tripartite neuropil (PL1b) (Figures 4b and 6a). The smaller anterior-lateral eye (ALE) extends RCA only into the right (lateralmost) "finger" of the tripartite neuropil (AL1; Figures 4c and 6a), but some axons terminate posterior of the AL1 (Figures 4c' and 6a). Crossing of RCA from the different eyes was not observed, implying that each eye strictly serves its own visual neuropils (Figures 4a–c and 6a). Thus, PME and PLE send axons into two first-order visual neuropils, PM1a, PM1b, PL1a, and PL1b, while the ALE only sends axons into one first-order visual neuropil, the AL1 (Figure 4a–c). While PM1b, PL1b, and AL1 are connected to the region just anterior and ventral of the AB via long neurites that run along the outer rim of the protocerebrum, PM1a and PL1a are connected to the anterior MB via thick neurite tracts (Figures 3f-f',h and 6a).

In *P. tepidariorum*, there is only one pair of first-order visual neuropils of the secondary eyes (SecVN1), supplied by RCA of all secondary eyes as shown by Bodian stains and dye backfills (Figures 3e-e' and 4d-e'). While the RCA of the ALE mostly terminates anterior-medially in the SecVN1, the termination sites of the PME RCA are more distributed throughout the neuropil and some terminate posteriorly and outside of the SecVN1 (Figures 4d-e' and 6b). Due to the small size of the secondary eyes, we were not able to trace the PLE RCA, but these likely terminate in the most lateral part of the SecVN1 (Figures 4e and 6b). A thin tract of neurites connects the SecVN1 directly to the AB, similar to the other species studied (Figures 3e-e' and 6b). Tubulin-immunostaining shows that further neurites originating from the SecVN1 run ventrally into the PN (Figure 3g-g'). Their exact termination site or origin (if they are ascending neurites) could not be determined.

3.4 | Arcuate body

In all four species investigated, the AB is a distinct crescent-shaped neuropil in the dorso-posterior region of the brain, directly adjacent to the soma cortex (Figures 2, 3c-d,e'-f', 8a, 9, and 14a). It consists of three distinct layers and contains an intricate arrangement of fine neurites that cross each other in a regular pattern (Figures 8a and 9b,d). In sagittal sections using Bodian stains or anti-tubulin immunolabeling, a group of neurites (likely primary neurites) arises in the soma cortex dorsal of the AB, passes through the AB, and projects into the central part of the PN (Figure 14). In all species examined, the AB is the termination site

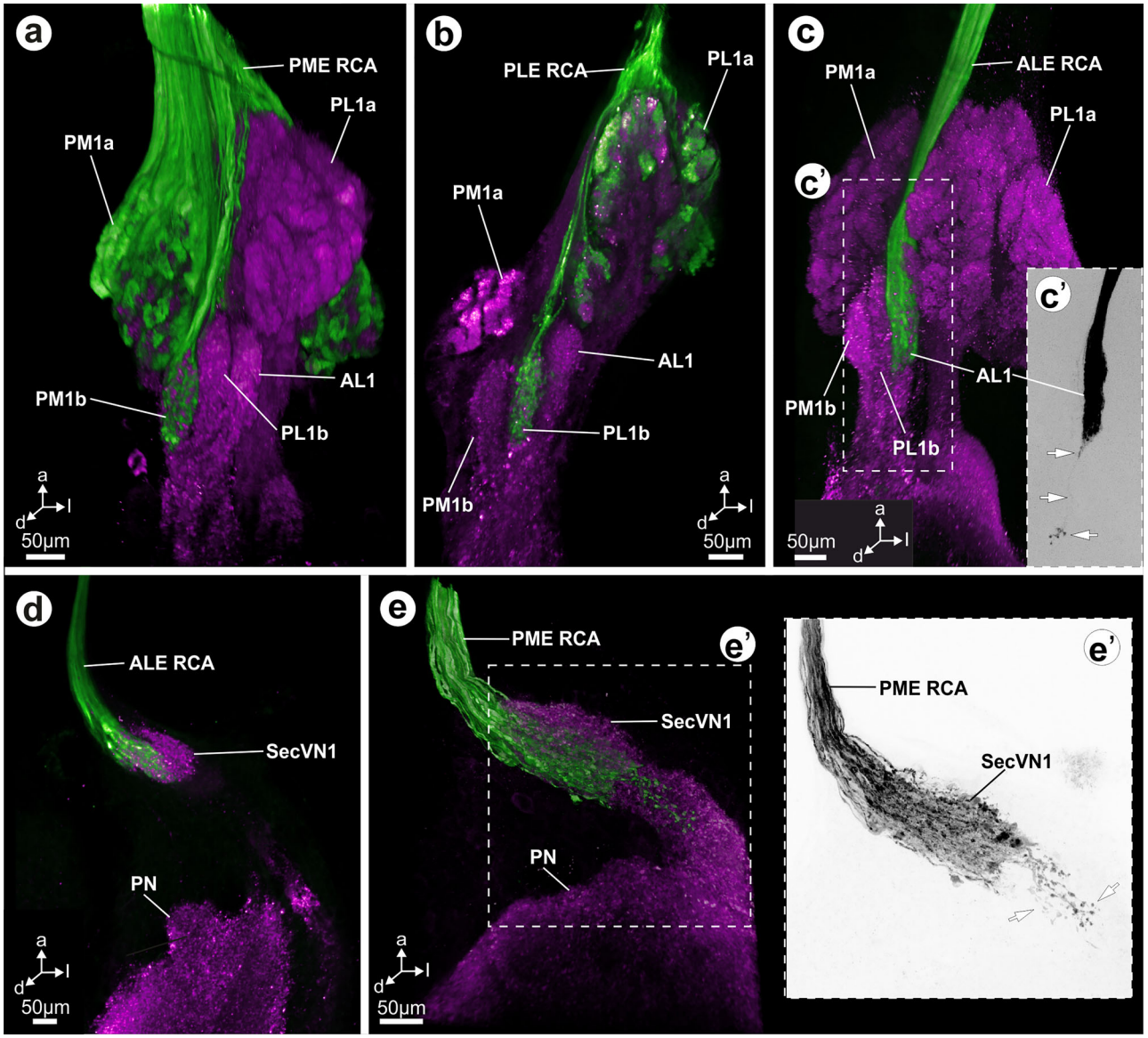

FIGURE 4 Maximum projections of image stacks (cLSM) showing synapsin immunoreactivity (magenta), and anterograde tracing of retinula cell axons (green) in the secondary eye visual pathway of *A. bruennichi* (a-c) and *P. tepidariorum* (d-e). (a) Most RCA of the PME terminate in the PM1a, while some terminate in the PM1b instead. (b) Most RCA of the PLE terminate in the PL1a, while some terminate in the PL1b instead. (c) RCA of the ALE terminate in the AL1. (c') Maximum intensity projection of the anterograde tracing of ALE RCA alone, reveals that some terminate posterior and just outside of the AL1. Termination sites highlighted by arrows. (d) RCA of the ALE terminate in the medial part of the roundish SecVN1. (e) RCA of the PME terminate in the SecVN1. (e') Maximum intensity projection of the anterograde tracing of PME RCARCA alone, reveals that some terminate posterior and just outside of the SecVN1. Termination sites highlighted by arrows. a, anterior; ALE, anterior lateral eyes; AL1, first-order visual neuropil of the anterior lateral eyes; d, dorsal; l, lateral; PLE, posterior lateral eyes; PL1a, first-order visual neuropil of the posterior lateral eyes a; PL1b, first-order visual neuropil of the posterior lateral eyes b; PME, posterior medial eyes; PM1a, first-order visual neuropil of the posterior median eyes a; PM1b, first-order visual neuropil of the posterior median eyes b; PN, protocerebral neuropil; RCA, retinula cell axon; SecVN1, first order visual neuropil of the secondary eyes.

of neurites from the visual neuropils AM2, PL1, AL1, and PM1 (PL1b and PM1b in *A. bruennichi*, see above; Figures 2b-d' and 3c-f'). The AB is further connected to the PN and the VNC via the protocerebro-dorsal tract (PCDt; see details below; Figure 9a,c,f). We did not detect any significant differences between the four species in the structure and connectivity of the AB.

3.5 | Mushroom bodies

Pardosa amentata possesses prominent, bilaterally paired MB, that can be subdivided into three structures: the cup-shaped MBd, the mushroom body pedunculus (MBp), and the mushroom body haft (MBh; Figures 3a,c, 5a, 7a,b, and 14a). The MB are connected to each other

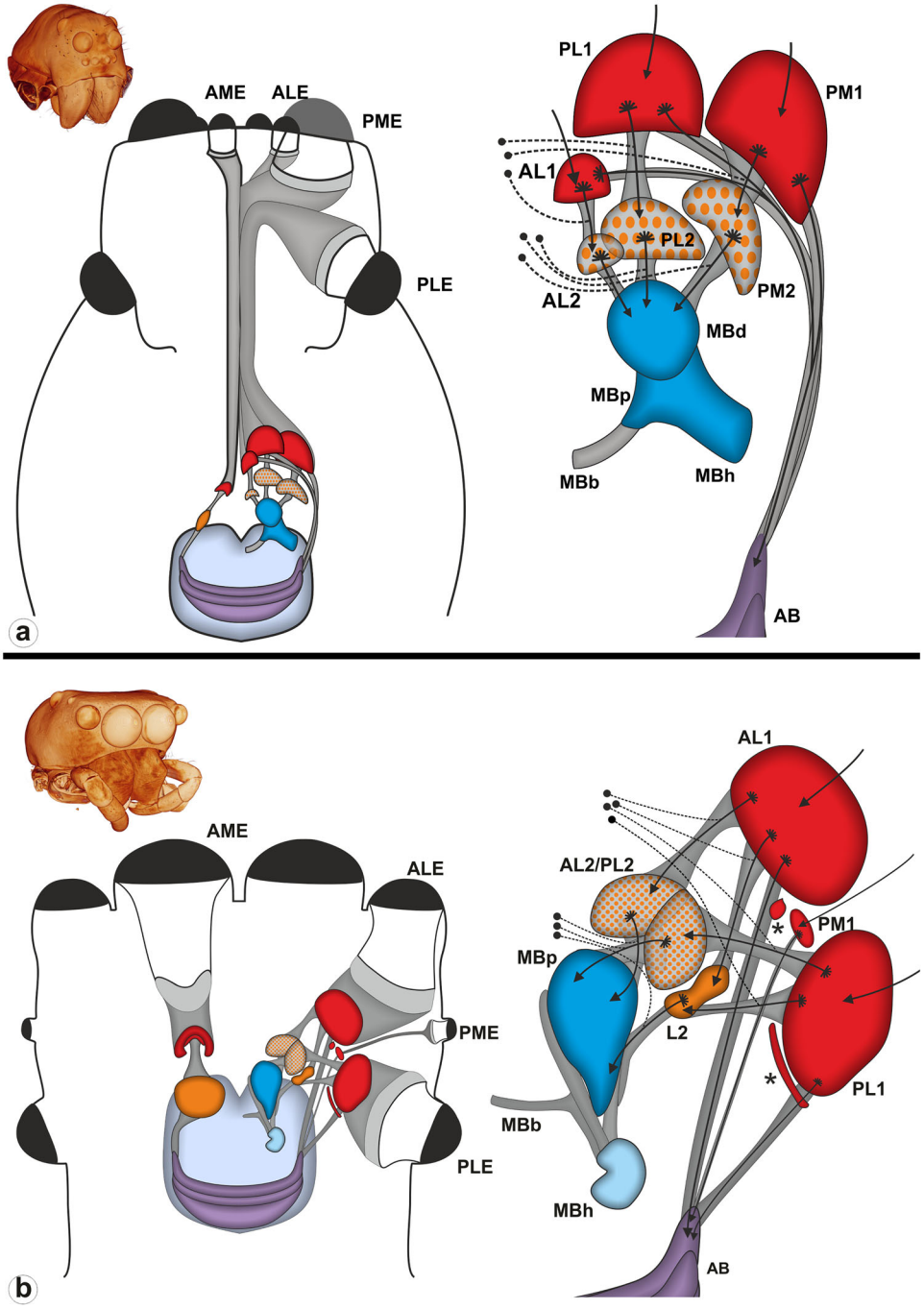

FIGURE 5 Schematic representations of the principal and secondary eye visual pathways in the brains of (a) *P. amentata* and (b) *M. muscosa*. Only part of each tract is drawn for clarity, tracts do not originate in different parts of the primary neuropils. Insets top left: Three-dimensional volume rendering of the prosomata of (a) *P. amentata* and (b) *M. muscosa*, based on microCT analysis. Filled black circles indicate somata with known positions, dotted lines represent primary neurites, and arrows indicate the assumed direction of information flow. Asterisks mark neuropilar subregions of first-order neuropils (AL1x and PL1x) in M. muscosa. AB, arcuate body; AL1, first-order visual neuropil of the anterior lateral eyes; AL2, second-order visual neuropil of the anterior lateral eyes; AL2/PL2, second-order visual neuropil of anterior lateral and posterior lateral eyes; ALE, anterior lateral eye; AME, anterior median eyes; L2, shared second-order visual neuropil of the anterior lateral and posterior lateral eyes; MBb, mushroom body bridge; MBd, mushroom body head; MBh, mushroom body haft; MBp, mushroom body pedunculus; PL1, first-order visual neuropil of the posterior lateral eyes; PL2, second-order visual neuropil of the posterior lateral eyes; PLE, posterior lateral eye; PME, posterior median eye; PM1, first-order visual neuropil of the posterior median eyes; PM2, second-order visual neuropil of the posterior median eyes. (b) Modified from Steinhoff et al. (2020).

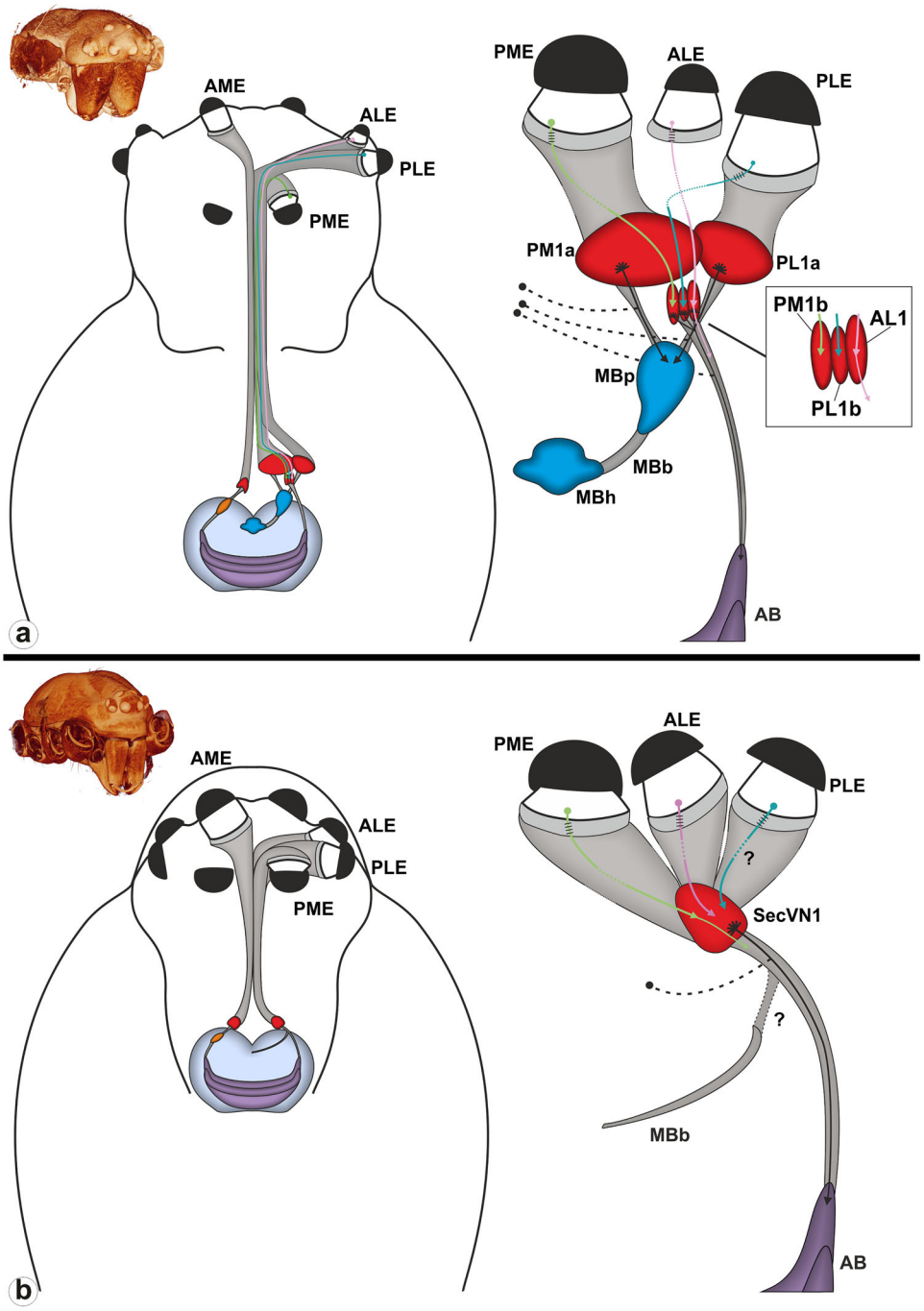

FIGURE 6 Schematic representations of the principal and secondary eye visual pathways in the brains of (a) *A. bruennichi* and (b) *P. tepidariorum*. Insets top left: Three-dimensional volume rendering of the prosomata of (a) *A. bruennichi* and (b) *P. tepidariorum*, based on microCT analysis. Filled black circles indicate somata with known positions, dotted lines represent primary neurites, and arrows indicate the assumed direction of information flow. AB, arcuate body; AL1, first-order visual neuropil of the anterior lateral eyes; ALE, anterior lateral eye; AME, anterior median eyes; MBb, mushroom body bridge; MBh, mushroom body haft; MBp, mushroom body pedunculus; PL1a, first-order visual neuropil of the posterior lateral eyes a; PL1b, first-order visual neuropil of the posterior lateral eyes b; PLE, posterior lateral eye; PME, posterior median eye; PM1a, first-order visual neuropil of the posterior median eyes a; PM1b, first-order visual neuropil of the posterior median eyes b; SecVN1, first order visual neuropil of the secondary eyes.

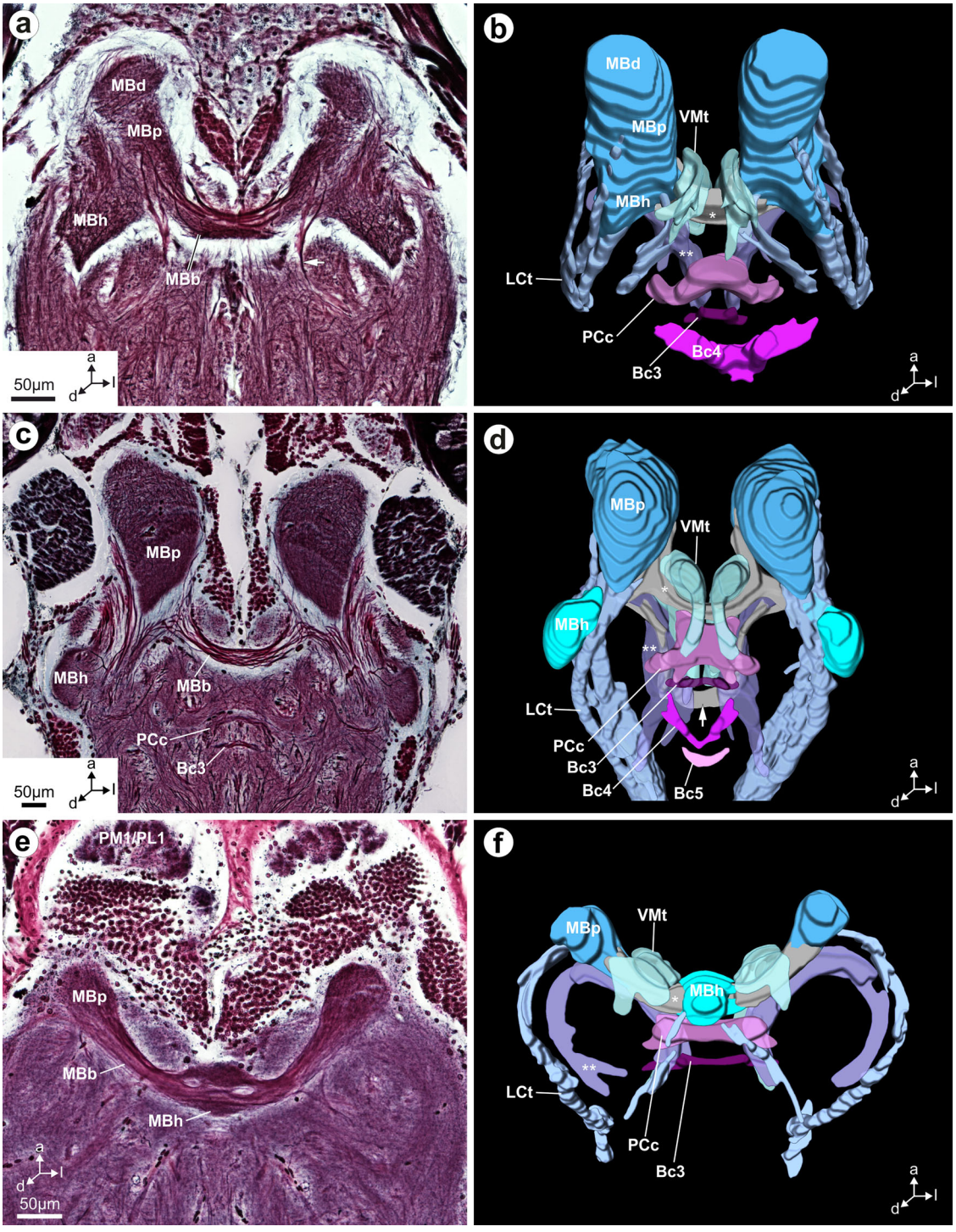

FIGURE 7 Mushroom bodies and brain tracts. (a, c, e) Bodian-stained sections. (b, d, f) Three-dimensional reconstructions based on serial Bodian-stained sections. (a-b) In *P. amentata* the MB consist of a MBd, MBp, and MBh and are connected to their bilateral counterpart via a thick MBb (*). While the LCt connects the MB to the VNC, the PCVt (**) forms an arch beneath the MB. The VMt crosses over the MBb. Further commissures in the PN are the PCc Bc3 and Bc4, which are all situated posterior of the MB. (c-d) In *M. muscosa* the MB consist of the MBp and the MBh. There is an additional protocerebral commissure, the Bc5. Arrow points to the MBb2. (e-f) In *A. bruennichi*, the MBh is situated medially. A Bc4 is not present. a, anterior; AB, arcuate body; Bc3, brain commissure 3; Bc4, brain commissure 4; Bc5, brain commissure 5; d, dorsal; l, lateral; LCt, lateral cerebral tract; * = MBb, mushroom body bridge; MBb2, mushroom body bridge 2; MBd, mushroom body head; MBh, mushroom body haft; MBp, mushroom body pedunculus; PCc, protocerebral commissure; ** = PCVt, protocerebro-ventral tract; PM1/PL1, first-order visual neuropil of the posterior median and posterior lateral eyes; VMt, ventral median tract.

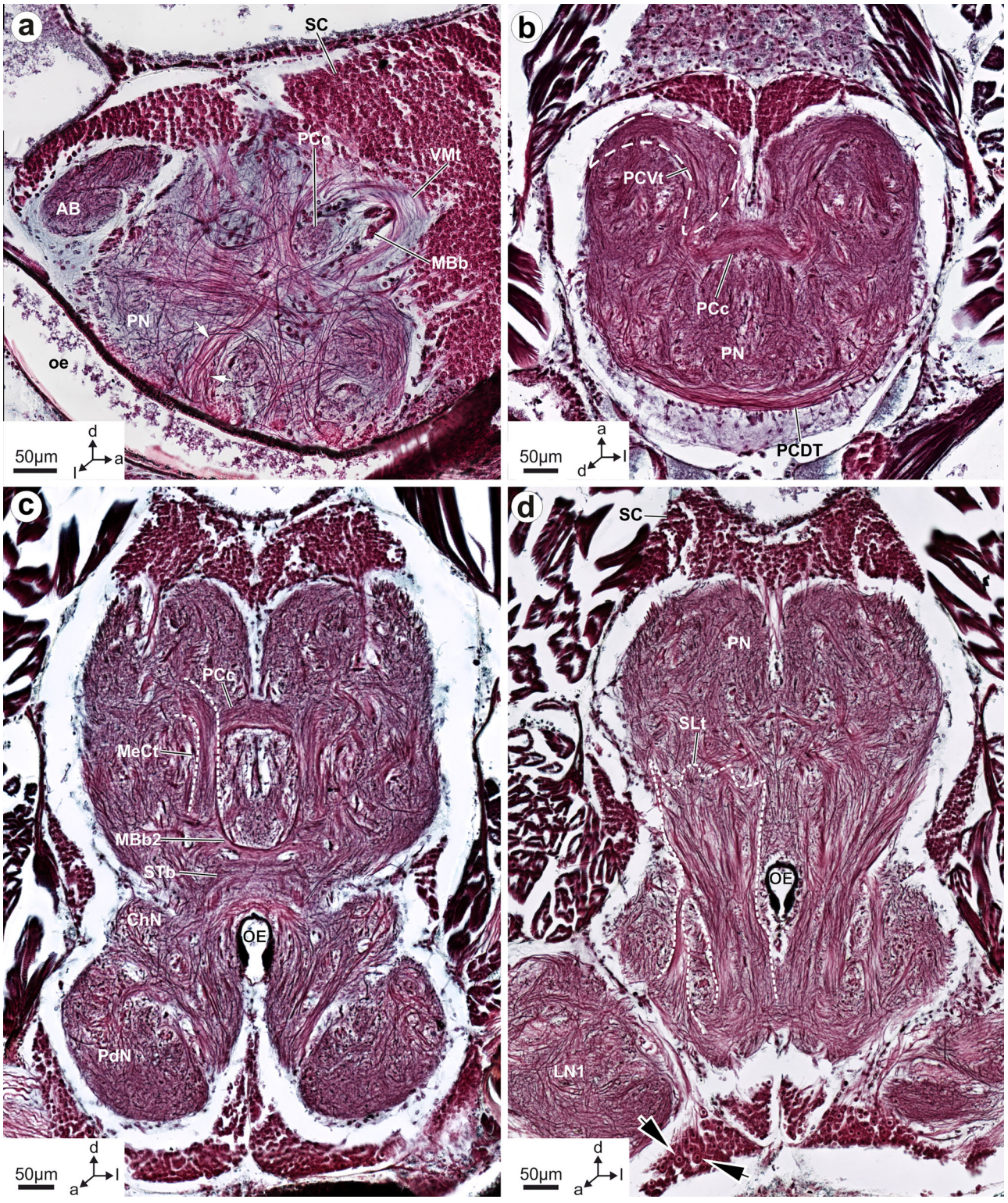

FIGURE 8 Bodian-stained sections reveal protocerebral tracts and connections between protocerebrum and VNC in *P. amentata*. (a) The VMt curves around the MBb and the PCc. Arrows point to long neurites within the PN, likely contributing to the MeCt. (b) PCVt forms an arch below the MB, the PCc consist of thin neurites and a central neuropilar structure. The PCDt is situated just below the AB. (c) Neurites that contribute to the thin MBb2 are embedded in the MeCt, which extends dorsally into the PN, passing the PCc. The STb neuropil forms an arch above the oe. OE is bordered by the ChN, below which is the PdN. (d) The SLt forms a massive tract connecting the VNC with the brain. Arrows point to giant somata that send their neurites into the VNC. AB, arcuate body; a, anterior; ChN, cheliceral neuropil; d, dorsal; l, lateral; LN, leg neuropil; MBb, mushroom body bridge; MBb2, mushroom body bridge 2; MeCt, median cerebral tract; OE, esophagus; PCc, protocerebral commissure; PCDt, protocerebro-dorsal tract; PCVt, protocerebro-ventral tract; PdN, pedipalpal neuropil; PN, protocerebral neuropil; SC, soma cortex; STb, stomodeal bridge; VMt, ventral median tract.

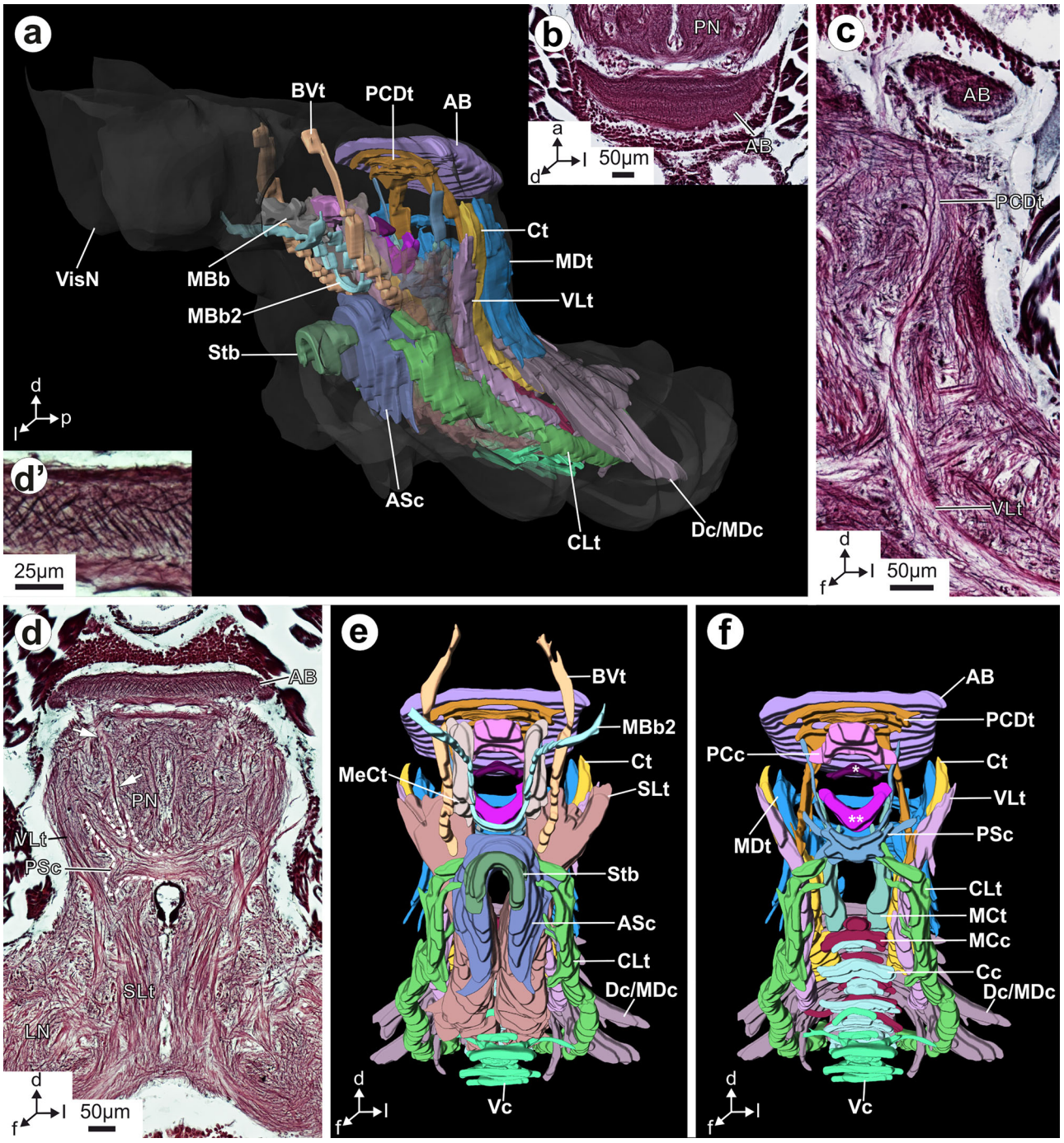

FIGURE 9 Tract system connecting the brain with the VNC in *P. amentata*. (a, e, f) Three-dimensional reconstructions based on serial Bodian-stained sections. (b, c, d, d') Bodian-stained sections. (a) CNS (transparent gray) with tracts, reconstruction of visual and VNC neuropils removed for clarity, SLt and MeCt transparent for clarity. (b) Intricate web of fine neurites in the AB. (c) PCDt connects to the AB and directly to the tract system of the VNC (specifically the VLt). (d) Long neurites connect the AB to the PSc (arrows). SLt passes next to the OE into the brain. (e) The ASc connects to the VNC; BVt sends neurites through the brain into the SLt. The MBb2 forms a commissure dorsal of the Stb and ASc. VNC commissures Dc/MDc and Vc are visible ventrally. (d') Enlarged image from d, showing fine neurites in the AB. (f) Same as (e), but Stb, ASc, MBb2, MeCt, BVt and SLt omitted to reveal more posterior located tracts. VNC commissures Vc, Dc/MDc, Cc and MCc are visible, VNC longitudinal tracts MDt, Ct, VLt, CLt and MCt curve upward into the brain. The PCDt connects the AB to the VNC and the PCc forms a thick dorsal commissure. Below the PCc are the Bc3 (*) and the Bc4 (**). In the postero-ventral PN is the PSc, with neurites extending into the dorsal PN. a, anterior; AB, arcuate body; ASc, anterior stomodeal commissure; * = Bc3, brain commissure 3; ** = Bc4, brain commissure 4; BVt, brain vertical tract; Cc, central commissure; CLt, centro-lateral tract; Ct, central tract; d, dorsal; Dc/MDc, dorsal and mid-dorsal commissures; f, frontal; l, lateral; LN, leg neuropil; MeCt, median cerebral tract; MBb, mushroom body bridge; MBb2, mushroom body bridge 2; MCc, mid-central commissure; MCt, mid-central tract; MDt, mid-dorsal tract; p, posterior; PCc, protocerebral commissure; PCDt, protocerebro-dorsal tract; PN, protocerebral neuropil; PSc, posterior stomodeal commissure; SLt, sensory longitudinal tract; Stb, stomodeal bridge; Vc, ventral commissure; VisN, visual neuropils; VLt, ventro-lateral tract.

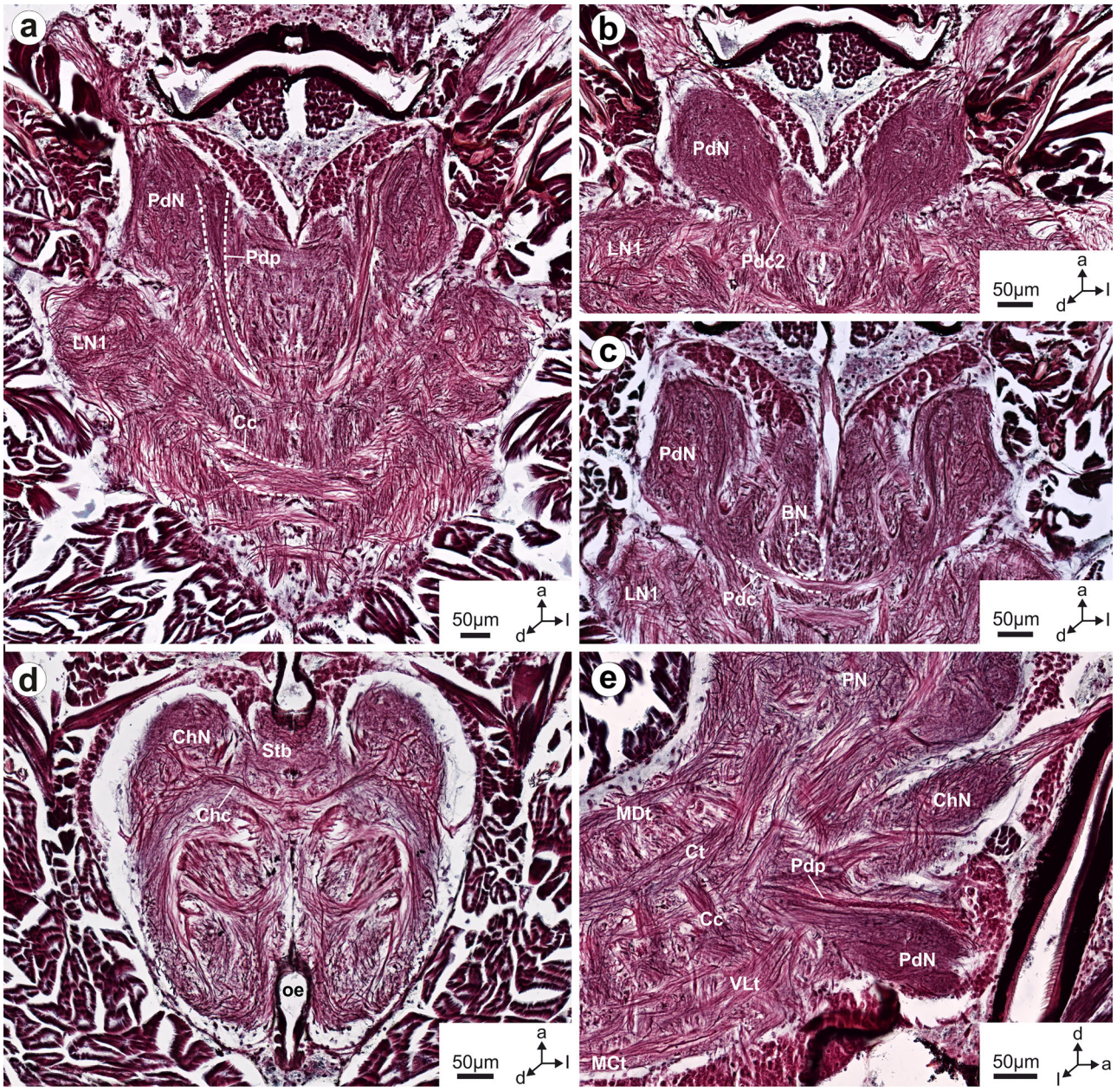

FIGURE 10 Bodian-stained sections of cheliceral and pedipalpal neuropils and tracts in *P. amentata*. (a) Pdp connects PdN with the SLt, the first LN is visible and part of the Cc. (b) The Pdc2 is located in a ventral position, connecting the two bilaterally paired PdN. (c) The BN consists of conspicuous columns that are arranged from dorsal to ventral and border the Pdc, which is situated dorsal of the Pdc2. (d) The Chc connects the two bilaterally paired ChN. The Stb surrounds the OE dorsally. (e) Neurites connect the PdN and ChN with VNC tracts. Prominent longitudinal VNC tracts are the MDt and CTt, part of the Cc, VLt and MCt are also visible. a, anterior; BN, Blumenthal neuropil; Cc, central commissure; Chc, cheliceral commissure; ChN, cheliceral neuropil; Ct, central tract; d, dorsal; l, lateral; LN1, leg neuropil of the first pair of legs; MCt, mid-central tract; MDt, mid-dorsal tract; PdN, pedipalpal neuropil; Pdc, pedipalpal commissure; Pdc2, pedipalpal commissure 2; Pdp, pedipalpal projection; PN, protocerebral neuropil; VLt, ventro-lateral tract.

by a thick commissure (mushroom body bridge, MBb) that forms an arch across the midline of the brain and enters the MBp from the posterior (Figures 3c, 5a, and 7a,b). A second, much thinner commissure consisting of a few long neurites (MBb2) is situated posterior-ventrally of the MB, embedded within the PN (Figures 8b and 9a,e). The neurites that compose the MBb2 are part of the median cerebral tract (MeCt; see below) and enter the MBp from ventrally (Figure 9a,e). The MBb2 could only be detected in frontal Bodian-stained sections, likely due to the fact that it is very thin. In *M. muscosa*, however, the MBb2 is composed of more neurites and can be distinguished in both horizontal and frontal Bodian-stained sections (Figure 7d). An MBd is not detectable in *M. muscosa* and the MBh does not form a continuous neuropil with the MBp as was found for *P. amentata* (Figure 7c,d; cf. also Steinhoff et al., 2020).

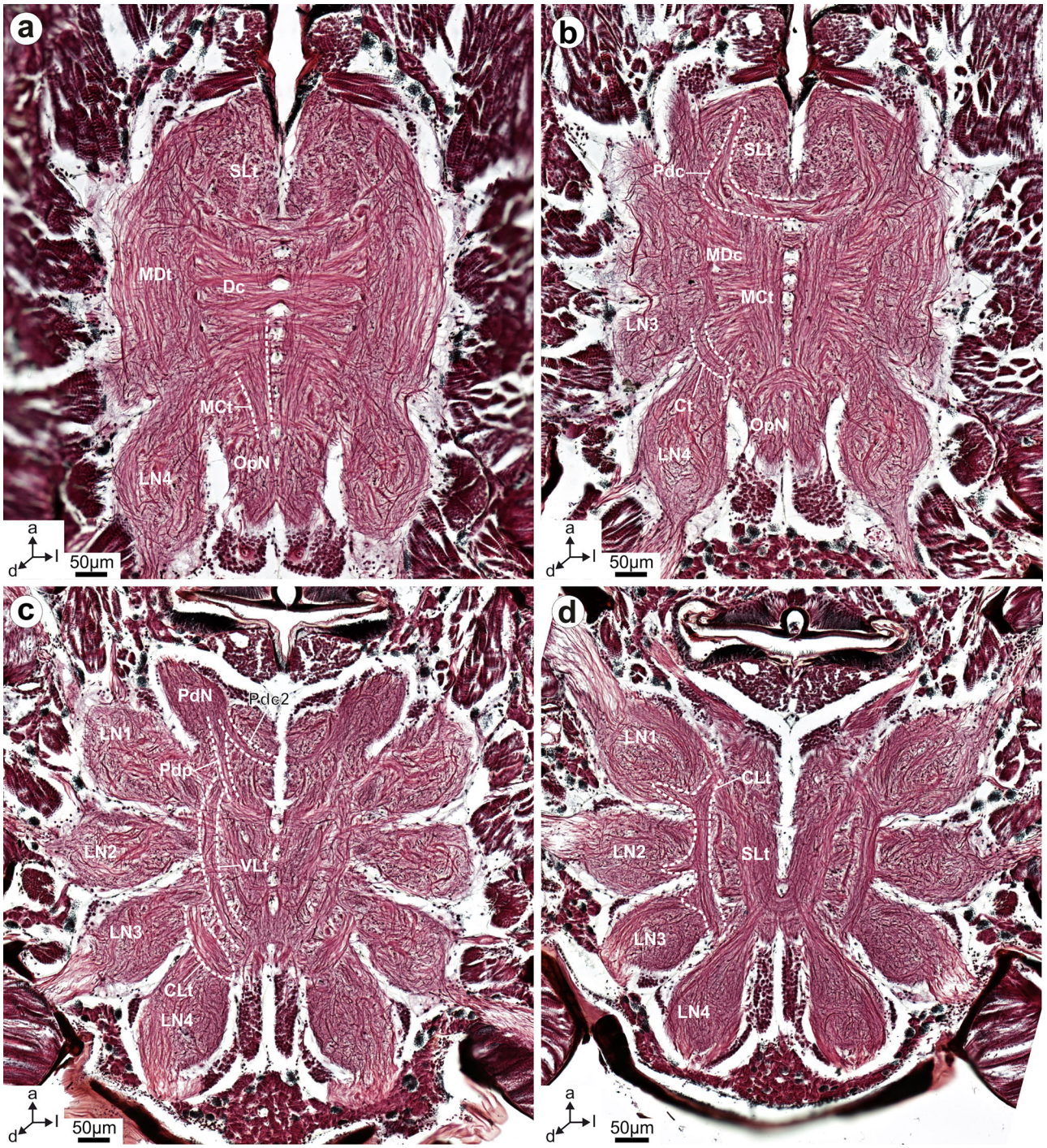

FIGURE 11 Bodian-stained sections showing major tracts in the VNC of *P. tepidariorum*, shown exemplary for all species studied here. (a) The MDt is the dorsalmost and largest longitudinal tract in the VNC. The SLt, which runs ventrally, can be seen anterior where it curves upward to enter the brain. The Dc connects the two halves of the VNC, the posterior part of the MCt is also visible. The posterior part of the VNC is formed by the LN4 and the OpN. (b) The MCt is the centralmost longitudinal tract in the VNC, part of the Ct is also visible. The Pdc is situated just beneath the MCt. (c) CLt and VLt are located more ventral in the VNC. The 4 LN send neurites into the central part of the VNC. The Pdp and Pdc2 arise in the PdN. (d) The SLt consists of thin neurites and stains darker than the other longitudinal tracts, connections between LN1-3 and the CLt and between LN4 and the SLt are visible. a, anterior; CLt, centro-lateral tract; Ct, central tract; d, dorsal; Dc, dorsal commissure; l, lateral; LN1-4, leg neuropil 1–4; MCt, mid-central tract; MDt, mid-dorsal tract; MDc, mid-dorsal commissure; OpN, opisthosomal neuropil; Pdc, pedipalpal commissure; Pdc2, pedipalpal commissure 2; Pdp, pedipalpal projection; SLt, sensory longitudinal tract; VLt, ventro-lateral tract.

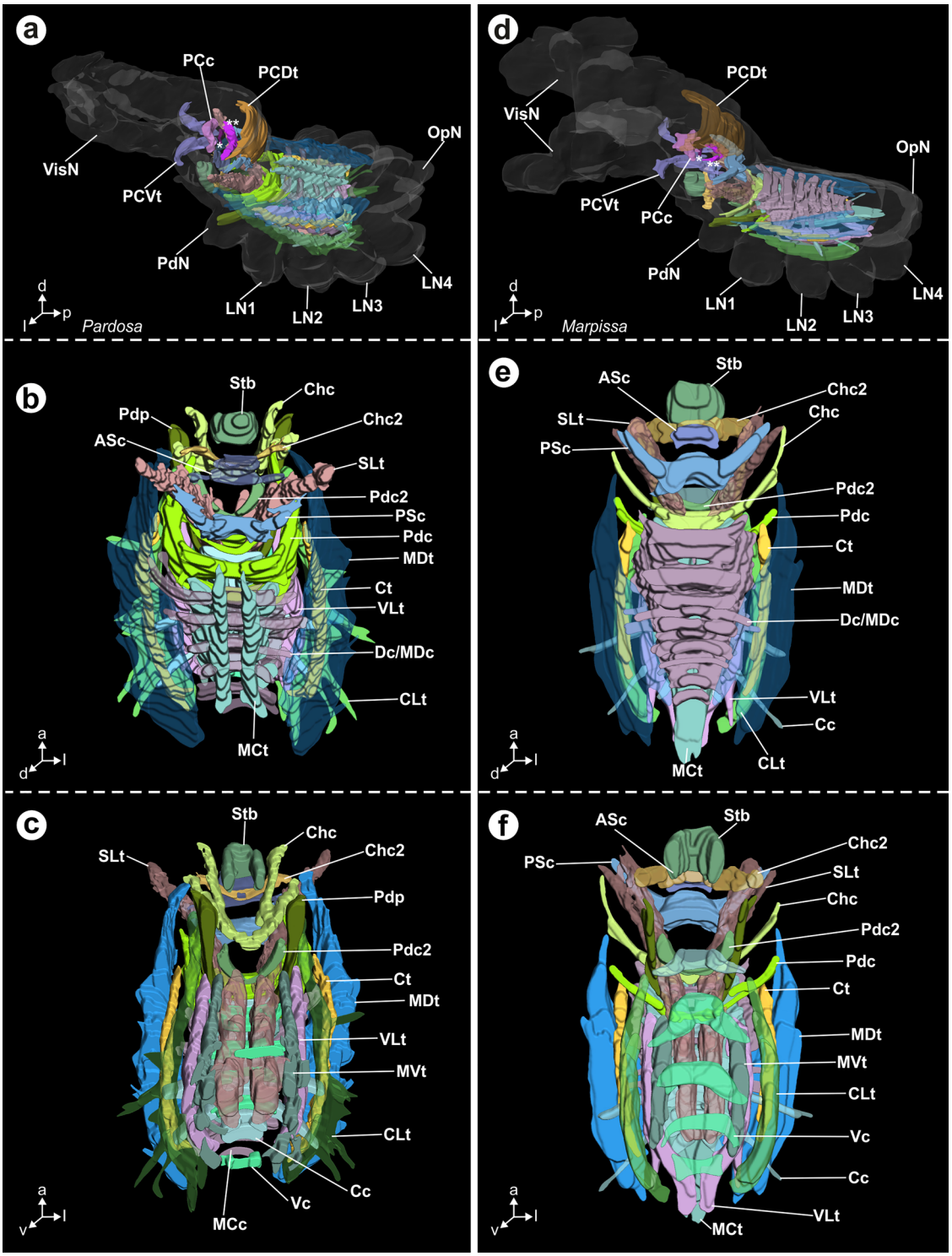

FIGURE 12 CNS tracts in *P. amentata* (a-c) and *M. muscosa* (d-f). (a-f) Three-dimensional reconstructions based on serial Bodian-stained sections. (a, d) CNS (transparent gray) with tracts, reconstruction of visual neuropils, most protocerebral tracts and VNC neuropils removed for clarity. (b-c,e-f) Ventral protocerebral, all deuto- and tritocerebral and all VNC tracts in dorsal (b,e) and ventral (c,f) view. a, anterior; ASc, anterior stomodeal commissure; * = Bc3, brain commissure 3; ** = Bc4, brain commissure 4; Cc, central commissure; Chc, cheliceral commissure; Chc2, cheliceral commissure 2; CLt, centro-lateral tract; Ct, central tract; d, dorsal; Dc/MDc, dorsal and mid-dorsal commissures; f, frontal; l, lateral; LN1-4, leg neuropil 1–4; MCt, mid-central tract; MCc, mid-central commissure; MDt, mid-dorsal tract; MVt, mid-ventral tract; OpN, opisthosomal neuropil; p, posterior; PCc, protocerebral commissure; PCDt, protocerebro-dorsal tract; PCVt, protocerebro-ventral tract; Pdc, pedipalpal commissure; Pdc2, pedipalpal commissure 2; PdN, pedipalpal neuropil; Pdp, pedipalpal projection; PSc, posterior stomodeal commissure; SLt, sensory longitudinal tract; Stb, stomodeal bridge; Vc, ventral commissure; VisN, visual neuropils; VLt, ventro-lateral tract.

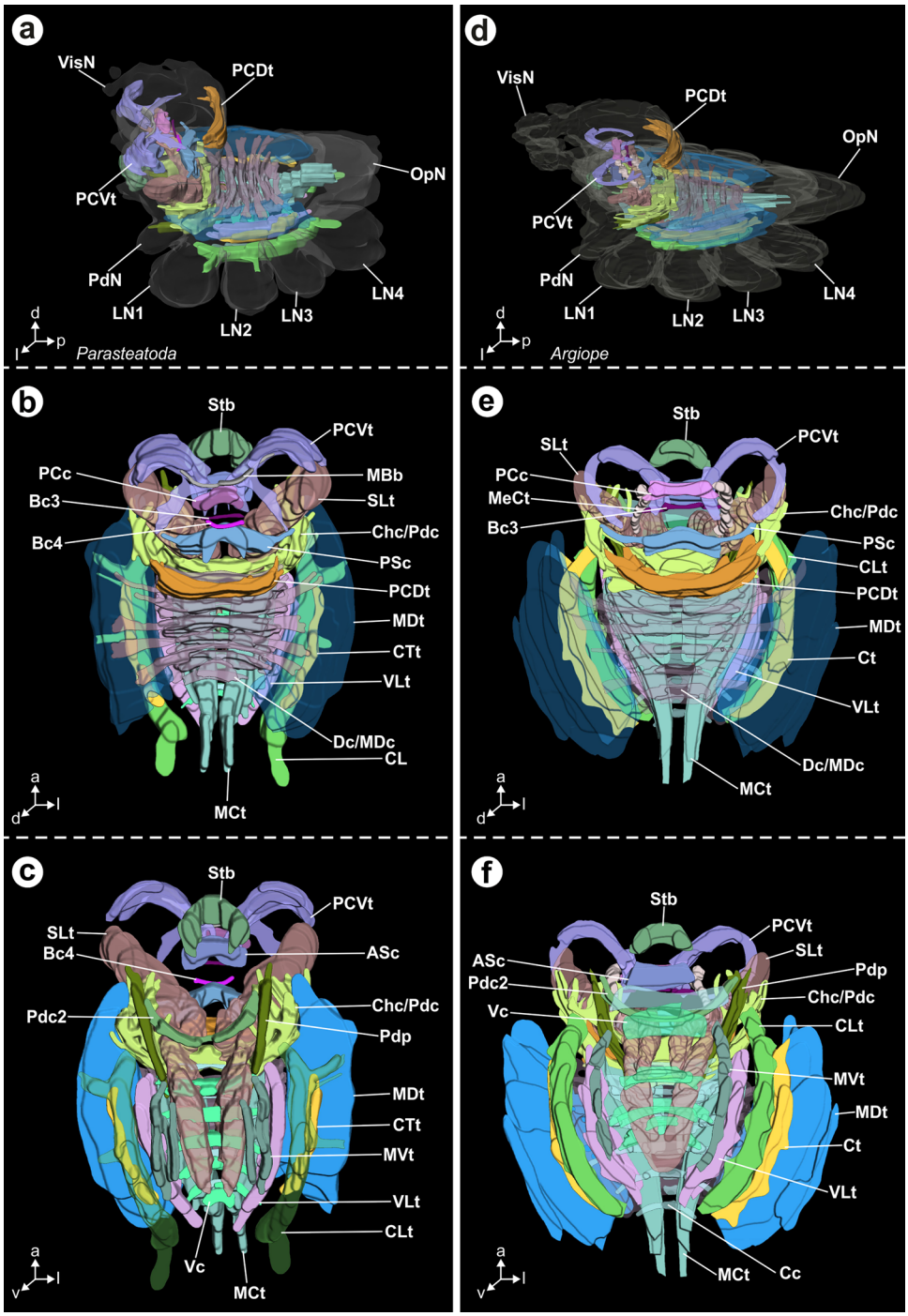

FIGURE 13 CNS tracts in *P. tepidariorum* (a–c) and *A. bruennichi* (d–f). (a–f) Three-dimensional reconstructions based on serial Bodian-stained sections. (a, d) CNS (transparent gray) with tracts, reconstruction of visual neuropils, most protocerebral tracts and VNC neuropils removed for clarity. (b-c,e-f) Most protocerebral, all deuto- and tritocerebral and all VNC tracts in dorsal (b,e) and ventral (c,f) view. a, anterior; ASc, anterior stomodeal commissure; Bc3, brain commissure 3; Bc4, brain commissure 4; Cc, central commissure; Chc/Pdc, cheliceral and pedipalpal commissure; CLt, centro-lateral tract; CTt, central tract; d, dorsal; Dc/MDc, dorsal- and mid-dorsal commissure; f, frontal; l, lateral; LN1-4, leg neuropil 1–4; MeCt, median cerebral tract; MBb, mushroom body bridge; MCt, mid-central tract; MCc, mid-central commissure; MCt, mid-central tract; MDt, mid-dorsal tract; MVt, mid-ventral tract; OpN, opisthosomal neuropil; p, posterior; PCc, protocerebral commissure; PCDt, protocerebro-dorsal tract; PCVt, protocerebro-ventral tract; PdN, pedipalpal neuropil; Pdp, pedipalpal projection; PSc, posterior stomodeal commissure; SLt, sensory longitudinal tract; Stb, stomodeal bridge; Vc, ventral commissure; VisN, visual neuropils; VLt, ventro-lateral tract.

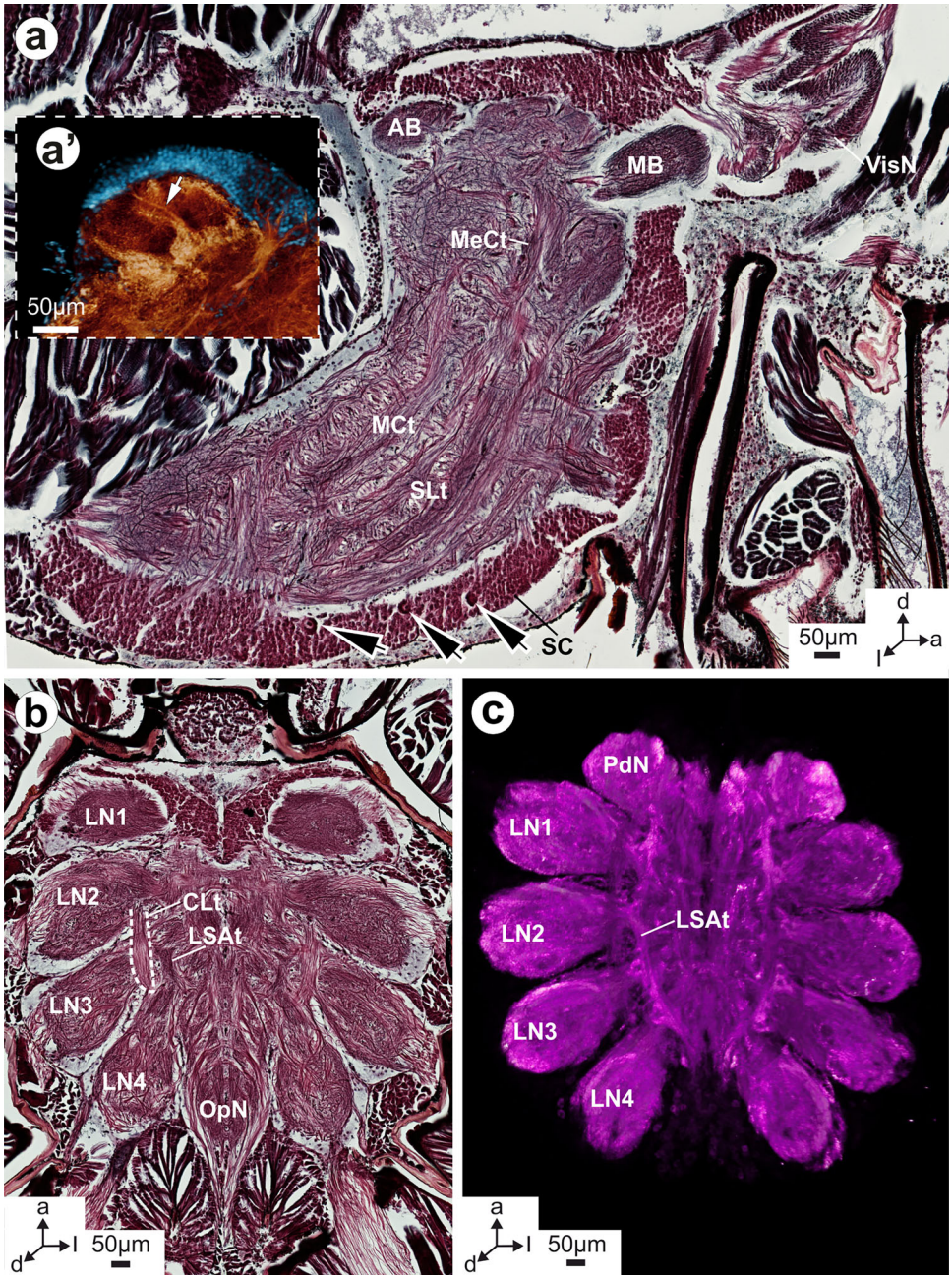

FIGURE 14 Tracts and neuropilar structures in the VNC of *P. amentata*. (a, b) Bodian-stained sections. (a) The MeCt connects the dorsal protocerebrum to the VNC. The SLt is visible as a thick tract with thin and dark-stained neurites, ventral of the MeCt. (a') Maximum projection of image stacks (cLSM) showing tubulin-immunoreactivity (gold) and nuclear marker (blue). Arrow points to neurites passing through the AB into the PN. (b) The OpN is heavily innervated by neurites projecting from and to the opisthosoma. Part of the CLt is visible and the LSAt is a neuropilar structure in the central part of the VNC. (c) Maximum projection of image stacks (cLSM) showing synapsin immunoreactivity (magenta). The LSAt spans the VNC from posterior to anterior. a, anterior; AB, arcuate body; d, dorsal; l, lateral; LN1-4; leg neuropils 1–4; LSAt, longitudinal sensory association tract; MB, mushroom bodies; MCt, mid-central tract; MeCt, median cerebral tract; PdN, pedipalpal neuropil; SC, soma cortex; SLt, sensory longitudinal tract; VisN, visual neuropils.

The MB in *A. bruennichi* consist of a drop-shaped MBp that shows strong synapsin immunoreactivity, a thick MBb containing large neurites, and a single roundish neuropilar structure, located in the center of the bridge on the midline of the brain, which we interpret as the MBh due to its direct connection to the MB (Figures 3f', h, 6a, and 7e,f). We did not detect an MBb2, but there are a few thin, long neurites projecting from the MBh into the central PN (Figure 7f). In *P. tepidariorum*, no MB-like neuropil could be detected by either immunostaining or Bodian staining. However, there is a thin commissure crossing the brain's midline, which we putatively interpret as MBb (Figures 3g' and 13b). An MBb2 is not present in *P. tediparium*.

3.6 | Protocerebral tracts

Apart from the visual neuropils, the protocerebrum in all species investigated consists of a central neuropil (PN), traversed by commissures that connect the different neuropils with each other, as well as prominent longitudinal tracts connecting the higher order neuropils AB and MB with the VNC. While several of the longitudinal tracts could be reconstructed from Bodian-stained serial sections, the exact connections of the commissures are not always clear. They are characterized here and synonymized between the different species based on their position and relative size. In *P. amentata*, we detected four brain commissures, which are: the anterior and posterior stomodeal commissures (ASc and PSc) and two commissures similar in size, both situated posterior to the stomodeal bridge neuropil (Stb) and bordering the PN dorsally and the esophagus ventrally (Figures 9a,d–f and 12a–c). The Stb is located just dorsally of the esophagus, enveloping it laterally and thus forming a horseshoe shape (Figures 8c, 9a,e, 10d, and 12a–c). The ASc consists of neurites that curve downward and form two thick tracts that reach the ventral part of the VNC and connect to the centro-lateral tract (CLt, see below; Figures 9a,e and 12b). The neurites making up the PSc, on the other hand, curve upward where they split up into individual neurites that reach both the lateral- and dorsalmost parts of the PN and connect the PSc directly to the AB (Figures 9d,f and 12b). Dorsal of the PSc are the Bc3 and Bc4, both of which are considerably smaller than the ASc and PSc (Figures 7a,b, 9f, and 12a). While the Bc4 is composed of neurites directed toward the dorsal PN, the Bc3 consists of neurites directed toward the ventral PN (Figures 9f). The dorsalmost commissure in the PN is the PCc, which consists of thin neurites embedded in a neuropilar structure and is situated immediately posterior of the MBb (Figures 8a–c, 9f, and 12a). A prominent tract (MeCt) connects the PCc directly with the VNC and joins the sensory longitudinal tract (SLt, see below; Figures 8c, 9e, and 14a). The MeCt also extends to a region dorsal of the PCc, showing that it consists not only of neurites involved in the PCc, but also of neurites originating dorsolaterally of the PCc (Figure 8c). Anteriolateral of the MeCt is the brain vertical tract (BVt), a conspicuous bundle of neurites originating in the dorsal somata cluster and extending ventrally into the SLt (Figure 9a,e). Anterior of the PCc is the protocerebro-ventral tract, which forms two bilaterally paired arches below the MB that extend into the central PN (Figures 7b, 8b, and 12a). The ventral median tract (VMt) is formed by neurites that pass below the PCc and the MBb and cross over the latter, where they enter the dorsal PN (Figures 7b and 8a). The lateral cerebral tract (LCt) is the most laterally located tract in the protocerebrum and connects the MB to the VNC (Figures 3c and 7b). In *P. amentata*, the LCt divides into four different tracts, one of which connects to the MBh, one to the MBp, and two to the MBd (Figure 7b). The PCDt is located just below the AB and forms an arch anterior of the neurites from the secondary eye visual neuropils (Figures 8b, 9a,c,d,f, and 12a). The PCDt also has branches that connect it to the AB, the VNC and the central PN (Figures 8b, 9a,c,d,f, and 12a). The brain commissures in *M. muscosa* are very similar in size and shape to those of *P. amentata* (Figures 7d and 12d–f). However, there is an additional commissure not found in *P. amentata* (brain commissure five, Bc6), which is situated dorsal of the PSc, has a downward curved shape, and consists of thin, tightly adjoining neurites (Figure 7d). In *M. muscosa*, the LCt splits into three individual tracts instead of four (as in *P. amentata*), two of which are connected to the MBp and one of which contributes to the MBb, while none appears to be directly connected to the MBh (Figure 7c,d). In *A. bruennichi*, the LCt arises from the mid-central tract (MCt) of the VNC (see below), does not split up in the protocerebrum, and connects to the MBp (Figure 7f). There are a number of neurites that extend from the MBh toward the LCt and might contribute to the formation of the LCt, but we did not observe a direct connection (Figure 7f). We did not detect Bc4 in *A. bruennichi*. While the general architecture of the protocerebral tract system in *P. tepidariorum* resembles that of *P. amentata*, we did not detect an LCt as in all other investigated species.

3.7 | Cheliceral neuropil and Pedipalpal neuropil

The ChNs border and extend above the esophagus, while the PdNs are entirely situated below the esophagus in all investigated species. Both the ChNs and PdNs are connected by commissures. There are two pedipalpal commissures in all species examined (Figures 10b,c, 11b, 12, and 13). There is a single cheliceral commissure in *A. bruennichi* and *P. tepidariorum* (Figure 13), whereas *P. amentata* and *M. muscosa* possess two cheliceral commissures located above and below the esophagus (Figures 10d and 12b,c,e,f). In addition to the pedipalpal commissures, every species has a ventrally situated bundle of neurites projecting from the PdN into the VNC (Pdp) and terminating within the SLt (see below; Figures 10a,e, 11c, and 12a–d,f).

3.8 | The Ventral nerve cord

The anatomy of the VNC is remarkably similar in the investigated species. The central neuropil is dominated by six major longitudinal tracts and contralateral commissures between the LNs, which are embedded in a central association area (Figures 11, 12, 13, and 14). This general layout is fairly consistent with the description of the VNC in *C. salei* (Babu & Barth, 1984). There are six longitudinal tracts that traverse the VNC from the posterior OpN to the brain, where they enter the PN and then split up into smaller tracts (described above; Figures 8d, 9a,c–f, and 10e). The mid-dorsal tract is the most dorsal one. This tract occupies most of the dorsal VNC (Figures 9a,f, 10e, 11a, 12, and 13). The MCt is situated just below the dorsal commissure (Dc) and flanks the midline of the VNC (Figures 9f, 11a,b, 12a,b,d,e, 13, and 14a). It has a distinct, almost triangular shape, with the widest part oriented toward and extending into the brain (Figure 11b). Ventral to the MCt follow three similarly sized tracts that form the core of the VNC: the CLt followed by/dorsal of the slightly more medial central tract (Ct), which is dorsal of the ventro-lateral tract (VLt; Figures 9a,c,e,f, 10e, 11b,d, 12, and 13). The most ventrally located tract is the mid-ventral tract, which is situated just dorsally of the ventral somata cluster

(Figures 10e, 12c,f, and 13c,f). In addition to these major longitudinal tracts, we identified a large tract (SLt; known to receive sensory input in *C. salei*), located in the centralmost area of the VNC, anteriorly connecting to the protocerebrum, where it splits into smaller tracts (see above, Figures 8d, 9a,d,e, 11a,b,d, 12, 13, and 14a). The SLt is characterized by mostly small neurites, which in Bodian preparations are darker stained than the neurites of the other six longitudinal tracts (Figures 8d, 9d, 11d, and 14a). In addition to the longitudinal tracts, there is a longitudinal neuropilar structure, the lateral sensory association tract (LSAt), which shows strong anti-synapsin immunoreactivity in all investigated species (Figure 14c). While it is easy to distinguish the different longitudinal tracts, it is more difficult to tell apart the different groups of commissures, which are often stacked in close proximity and connect the bilaterally paired LNs and longitudinal tracts. We identified four distinct commissures (Dc, mid-Dc [MDc], central commissure [Cc] and ventral commissure [Vc]; Figures 9e,f, 10a,e, 11a,b, 12, and 13) in all four species and an additional fifth commissure (mid-Cc: MCc; Figures 9f and 12c) in *P. amentata* and *M. muscosa*. In all four species, the Dc and MDc are closely adjacent without longitudinal tracts in between (Figures 11a, 12b,d,e, and 13a,b,d,e), while the other commissures are more clearly separated (Figures 9f, 10e, 12c,f, and 13c,f). In *P. amentata* and *M. muscosa*, we detected a somewhat columnar-shaped neuropilar structure just below the esophagus and bordering the midline of the brain. This structure stains darker than the surrounding tissue in the Bodian preparations (Figure 10c). We tentatively interpret this structure as Blumenthal neuropil (BN). However, we could not confirm its presence in anti-synapsin immunolabeling of *P. amentata* and *M. muscosa* nor find it at all in *A. bruennichi* and *P. tepidariorum*.

3.9 | Comparative volumetric analysis of the CNS neuropils

The spider species investigated here differ in their relative investment in different neuropils (see pie charts in Figure 16 for information on comparative brain volumes). In all four species, the VNC makes up more than half of the CNS volume, but it is much larger in the web-building spiders than in the cursorial hunting spiders (73.3% in *A. bruennichi* and 76.5% in *P. tepidariorum*, compared to 63.8% in *P. amentata* and 55% in *M. muscosa*). Correspondingly, the brain is much larger in the cursorial hunting spiders than in the web-building spiders. While the cVNC has a similar proportional volume in all four species, the LN and the OpN are proportionally larger in the web-building hunters *A. bruennichi* and *P. tepidariorum* than in the cursorial hunting spiders *P. amentata* and *M. muscosa*. The LN is also considerably larger in *P. amentata* than in *M. muscosa*. Within the brain, the largest differences in proportional investment are found between cursorial and web-building spiders, with *P. amentata* and *M. muscosa* having much more nervous tissue dedicated to visual processing (visual neuropils and MB) than *A. bruennichi* and *P. tepidariorum*. However, there are also clear differences between the two cursorial hunters (*M. muscosa* has a much larger proportional visual brain area than *P. amentata*) and the two web-building hunters (*A. bruennichi* has more nervous tissue dedicated to visual processing than *P. tepidariorum*). Furthermore, the visual neuropils of the principal eyes (PrincVis) have the same proportional volume in *P. amentata* and *A. bruennichi*. We also found that the relative volumes of the PN are somewhat larger in the cursorial hunting spiders than in the web-building spiders, while the PdN is largest in *P. amentata*, followed by *A. bruennichi*, *M. muscosa*, and *P. tepidariorum*. There seems to be no difference in the proportional volume of the AB and the ChN.

4 | DISCUSSION

Comparative studies on the neuroanatomy of spiders have so far focused on the visual system, particularly the neuropils in the secondary eye visual pathway (Hanström, 1921; Long, 2021; Steinhoff et al., 2020). Web-building spiders were reported to have fewer and smaller visual neuropils than cursorial hunting spiders; however, with high variability between species (Hanström, 1921; Long, 2021; Steinhoff et al., 2020). Here, we have extended the scope of comparative neuroanatomical studies in spiders by performing a detailed analysis of all parts of the CNS. While we confirm that the most striking differences occur in the secondary eye visual pathway, we also find additional differences in the connectivity and relative volume of neuropils in the brain, and show that the anatomy of the VNC is remarkably conserved among spider species with different sensory ecologies (Figures 5, 6, 11, 13, and 16; Table 3).

4.1 | Soma cortex and cell types

Babu and Barth (1984) distinguished four distinct cell types in *C. salei* and the ones with the smallest diameter were termed "globuli cells" because of the association with the MB. However, Steinhoff et al. (2020) reported that in *M. muscosa*, the somata in the corresponding cell cluster were not smaller than other somata. We can now confirm this finding using Bodian stains for all four species investigated here. We found that the somata in the anterior part of the brain are more densely packed (Figure 14a), but we did not find a cluster of distinctly smaller somata as described for *C. salei* (Babu & Barth, 1984; Strausfeld & Barth, 1993). Either an anterior protocerebral cluster of smaller somata is specific to *C. salei*, or there is not any real size difference between "globuli cells" and other small somata. Instead, the differences may only be in packing density. It should be noted, however, that Bodian-stained material is not the current method of choice to assess cell size, and future studies could approach this specific question using better-suited methods. Babu and Barth (1984) furthermore described large motor- or interneurons that clearly correspond to the giant somata described here (Figures 8d and 14a).

4.2 | Visual system

The number of neuropils in the visual system and their connectivity in the principal eye pathway is the same in all spider species studied to

TABLE 3 Neuropils and major longitudinal and commissural tracts in the central nervous system (CNS) of *Cupiennius salei*, *Pardosa amentata*, *Marpissa muscosa*, *Argiope bruennichi*, and *Parasteatoda tepidariorum*. Based on this study and (for *C. salei*) on Babu and Barth (1984, 1989).

CNS structures	*C. salei*	*M. muscosa*	*P. amentata*	*A. bruennichi*	*P. tepidariorum*
VNC neuropilar structures					
BN	+	+?	+?	–	–
SLt (1–5)	+ 5 tracts	+ Single tract	+ Single tract	+ Single tract	+ Single tract
LN	+	+	+	+	+
LSAt	+	+	+	+	+
OpN	+	+	+	+	+
Dcb & Tcb neuropils					
ChN	+	+	+	+	+
PdN	+	+	+	+	+
Pcb neuropilar structures					
AB	+	+	+	+	+
AM1	+	+	+	+	+
AM2	+	+	+	+	+
MB	+	+	+	+	–
MBh	+	+	+	+ Medially	–
PN	+	+	+	+	+
SecVN1	+	+	+	+	+ Shared
SecVN2	+	+	+	–	–
Stb	+	+	+	+	+
Pcb longitudinal tracts					
BVt	?	+	+	+	+
LCt	+	+	+	+	–
MCt	+	+	+	+	+
PCDt	+	+	+	+	+
PCMt	+	?	?	?	?
PCVt	+	+	+	+	+
VMt	+	+	+	+	+
Pcb commissural tracts					
ASc	?	+	+	+	+
Bc3	?	+	+	+	+
Bc4	?	+	+	-	+
Bc5	?	+	-	-	-
MBb	+	+	+	+	+
MBb2	?	+	+	–	–
PCc	+	+	+	+	+
PSc	?	+	+	+	+
Dcb & Tcb tracts					
Chc	+	+	+	+ Connected to Pdc	+ Connected to Pdc
Chc2	?	+	+	–	–
Pdc	+	+	+	+ Connected to Chc	+ Connected to Chc
Pdc2	?	+	+	+	+

(Continues)

TABLE 3 (Continued)

CNS structures	*C. salei*	*M. muscosa*	*P. amentata*	*A. bruennichi*	*P. tepidariorum*
Pdp	?	+	+	+	+
VNC longitudinal tracts					
CLt	+	+	+	+	+
CTt	+	+	+	+	+
MCt	+	+	+	+	+
MDt	+	+	+	+	+
MVt	+	+	+	+	+
VLt	+	+	+	+	+
VNC commissural tracts					
Cc	+	+	+	+	+
Dc	+	+	+ Connected to MDc	+ Connected to MDc	+ Connected to MDc
MCc	+	+	+	–	–
MDc	+	+	+ Connected to Dc	+ Connected to Dc	+ Connected to Dc
Vc	+	+	+	+	+

Abbreviations: AB, arcuate body; AM1, first-order visual neuropil of the AME; AM2, second-order visual neuropil of the AME; ASc, anterior stomodeal commissure; Bc3, brain commissure 3; Bc4, brain commissure 4; Bc5, brain commissure 5; BN, Blumenthal neuropil; BVt, brain vertical tract; Cc, central commissure; Chc, cheliceral commissure; Chc2, cheliceral commissure 2; ChN, cheliceral neuropil; CLt, centro-lateral tract; CTt, central tract; Dc, dorsal commissure; Dcb, deutocerebrum; LCt, lateral cerebral tract; LNs, leg neuropils; LSAt, lateral sensory association tract; MB, mushroom bodies; MBb, mushroom body bridge; MBb2, mushroom body bridge 2; MBh, mushroom body haft; MCc, mid-central commissure; MCt, mid-central tract; MDc, mid-dorsal commissure; MDt, mid-dorsal tract; MVt, mid-ventral tract; OpN, opisthosomal neuropil; PCc, protocerebral commissure; PCDt, protocerebro-dorsal tract; PCMt, protocerebro-median tract; PCVt, protocerebro-ventral tract; Pdc, pedipalpal commissure; PdN, pedipalpal neuropil; Pdp, pedipalpal projection; PN, protocerebral neuropil; PSc, posterior stomodeal commissure; SLt, sensory longitudinal tract; SecVN1, first-order visual neuropils of the secondary eyes; SecVN2, second-order visual neuropils of all secondary eyes; Stb, stomodeal bridge; Tcb, tritocerebrum; Vc, ventral commissure; VLt, ventro-lateral tract; VMt, ventral median tract; VNC, ventral nerve cord.

date (Long, 2021; Steinhoff et al., 2020; Strausfeld et al., 1993). Considering the variation within the visual pathway of the secondary eyes, this is remarkable and suggests that the AME serve a similar function in all spider species that possess them. In Salticids and in *C. salei*, the AME are used for object recognition (Fenk et al., 2010; Land, 1972; Schmid, 1998). However, whether web-building spiders such as *A. bruennichi* and *P. tepidariorum* are capable of such behavioral performance remains to be tested.

The visual system of the secondary eyes in *P. amentata* is very similar in anatomy and connectivity to that of *C. salei* (Steinhoff et al., 2020; Strausfeld & Barth, 1993). In both species, all secondary eyes serve their own first- and second-order visual neuropils, before the information is sent on to the MB. Furthermore, all first-order visual neuropils are connected to the AB. Aside from the similarities, the AL1, PL1, and PM1 appear to be much more convoluted in *P. amentata* than in *C. salei* (this study, cf. with Babu & Barth, 1984; Steinhoff et al., 2020; Strausfeld & Barth, 1993), which probably increases the surface area of these neuropils. This aspect coincides with the fact that *C. salei* is strictly nocturnal and hunts prey mainly through vibratory cues (Barth & Seyfarth, 1979), while *P. amentata* hunts its prey during the day, when more visual information is available. The secondary eye visual system of the web-building hunter *A. bruennichi* is very different from all other visual systems described so far in spiders. While *A. bruennichi* has no second-order visual neuropils, the PME and the PLE have specialized retinula cells that project either into a neuropil that is linked to the MB (PM1a, PL1a) or another neuropil that connects to the AB (PM1b, PL1b). Yet, the ALE only connects to a single neuropil, which is linked to the AB (AL1), but some RCA project further into the PN and could potentially connect the ALE to the MB as well. Long (2021) reported the absence of second-order visual neuropils in the species *A. trifasciata* but misinterpreted the identity of the different first-order visual neuropils as three different structures, each serving one eye. It would be interesting to explore how the distinct photoreceptors are arranged in the retina and whether they sample the entire field of view or only part of it. The lack of a second-order visual neuropil implies that less intensely processed information is sent to the MB in this species. The quality of motion vision might thus be reduced, compared to spiders with second-order visual neuropils. In *P. tepidariorum*, all secondary eyes extend their RCA into a single visual neuropil (SecVN1) that is directly connected to the AB. We found that some PME RCA terminate posterior of the SecVN1, and these may connect further to other brain regions than the AB. We also discovered a potential MBb, indicating the possibility that the MB circuit is present in *P. tepidariorum* but reduced to such a degree that no neuropils are visible.

4.3 | The spider mushroom body

The mushroom body of spiders is clearly a higher order visual neuropil, as it receives input mainly from the second-order visual neuropils of

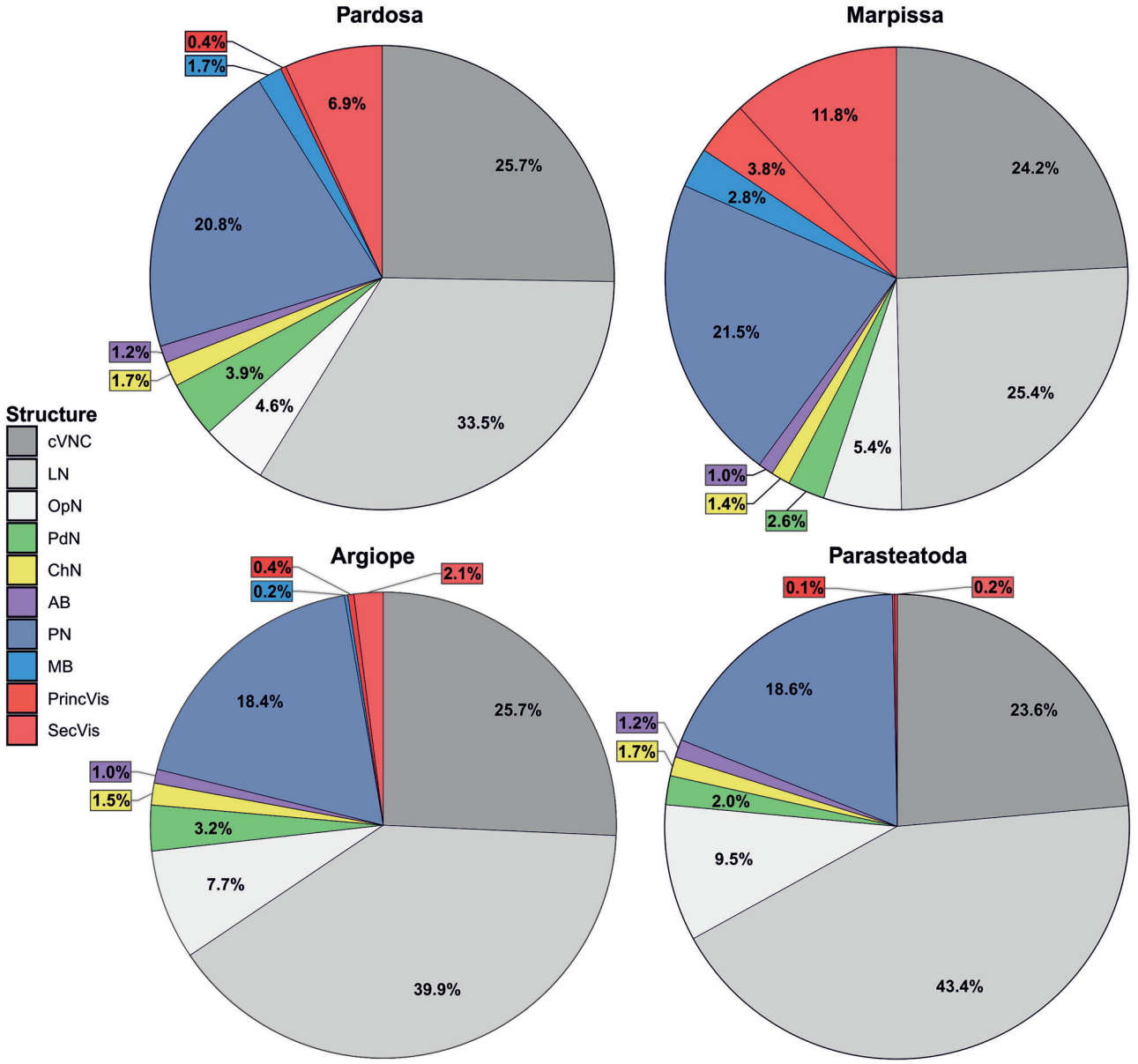

FIGURE 15 Pie charts showing the relative volumes of brain areas in proportion to the volume of the entire CNS in the studied species. AB, arcuate body; ChN, cheliceral neuropils; cVNC, central ventral nerve cord; LNs, leg neuropils; MB, mushroom bodies; OpN, opisthosomal neuropil; PdN, pedipalpal neuropil; PN, protocerebral neuropil; PrincVis, combined first- and second order visual neuropils of the principal eyes; SecVis, combined first- and second order visual neuropils of the secondary eyes.

the secondary eyes (Babu & Barth, 1984; Long, 2021; Steinhoff et al., 2020; Strausfeld & Barth, 1993, and cf. this study). Furthermore, we have shown here that *P. tepidariorum* does not possess any conspicuous mushroom body-like neuropils, which is also the case in other spider species and seems to be related to poor visual abilities and a stationary lifestyle (Long, 2021; Park et al., 2013). The obvious question that arises from these findings is whether the MB of spiders should be termed differently as has been done earlier (termed optical neuropil 3, ON3, in Strausfeld & Barth, 1993). This would avoid confusion with MB in insects that primarily process olfactory input. Wolff and Strausfeld (2015) regarded the MB to be lost in spiders but to be present in other arachnids. Unfortunately, this suggestion was not discussed or explained further by the authors but likely is based on the absence of expression of the DC0 and Leo proteins in the MB of the spiders they investigated. These markers, in contrast, are expressed in the MB of other arachnids such as amblypygids (Wolff & Strausfeld, 2015). However, earlier studies suggested, based on gene expression similarities, that the MB of insects and spiders are homologous (Doeffinger et al., 2010). Strausfeld (2012) argued that a switch in modality from olfaction to vision might have occurred. Developmental and gene expression studies might help to clarify this question. In the meantime, it seems appropriate to refer to the MB in spiders as "spider mushroom body" and point out that it differs at least functionally from the mushroom body of most insects and other arachnids.

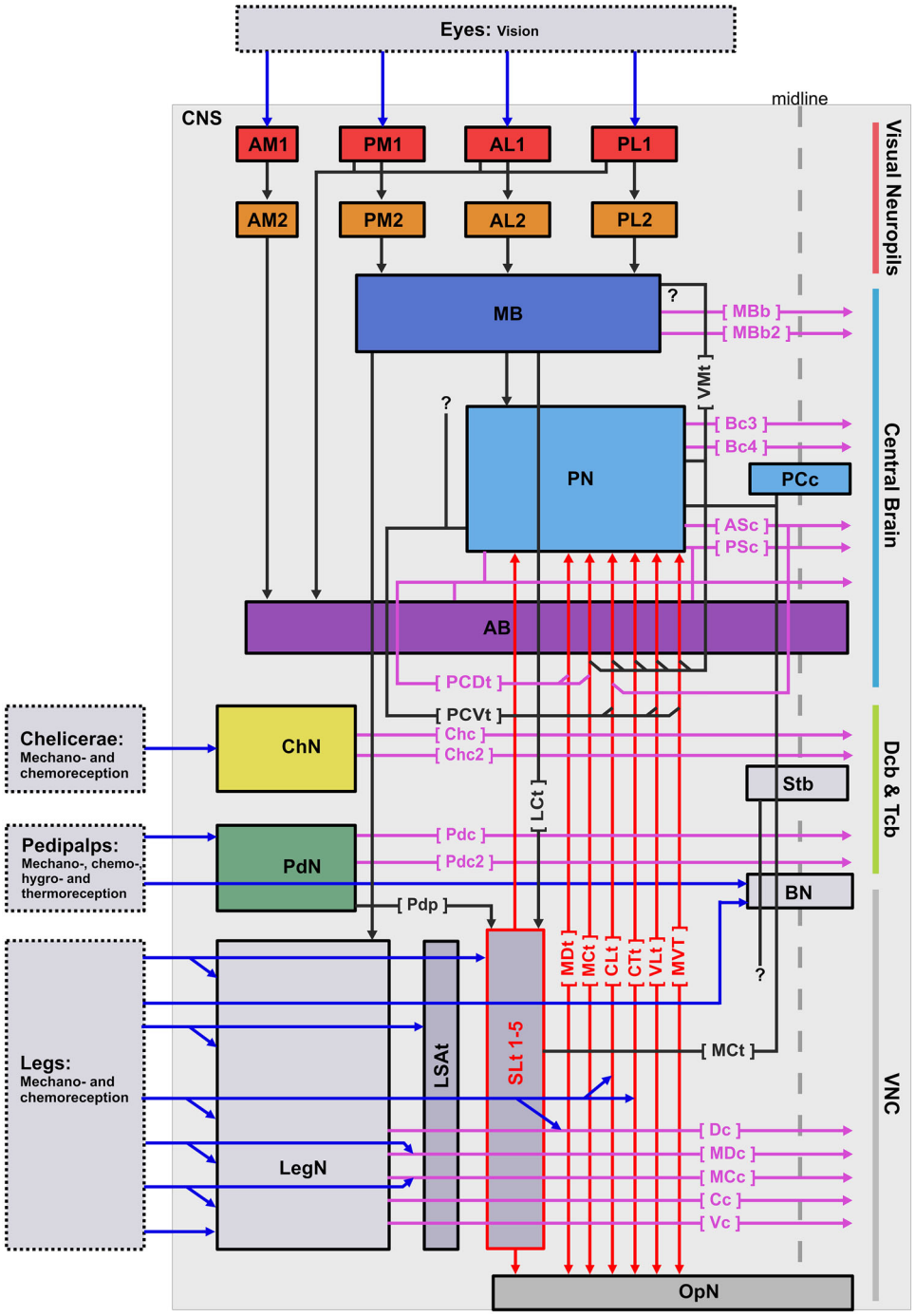

FIGURE 16 Schematic wiring diagram of the spider CNS. Visual system as in *C. salei* and *P. amentata*, for variation see Figures 4 and 5. Wiring of interneurons based on Babu and Barth (1984), Gronenberg (1989, 1990), and this study; innervation, central projection and termination pattern of sensory neurons based on Babu and Barth (1989), Anton and Tichy (1994), and this study. Blue lines represent sensory neurons, red lines represent longitudinal interneurons of the VNC, black lines represent interneurons of the brain, and pink lines represent commissural interneurons that cross the midline of the CNS. See list of abbreviations in the main text.

4.4 | Tracts in the protocerebrum

While the MBb and the PCc were described by Babu and Barth (1984) for *C. salei*, the other brain commissures discovered in this study (MBb2, Asc, Psc, Bc3, Bc4, Bc5) had not been detected in *C. salei* (Table 3). It is likely that these commissures contribute to smaller circuits that were not analyzed in the CNS of *C. salei* (Babu & Barth, 1984) since it seems unlikely that they are not also present in this species. The VMt was described as connecting to the MBp after crossing over the MBb in *C. salei* (Babu & Barth, 1984). We could not confirm this in any of

the four species studied here. It rather seems as if the VMt connects to the dorsal PN after crossing over the MBb (Figures 7 and 16). The PCDt was described as "entering the hafts" in *C. salei* (Babu & Barth, 1984), a pattern we could not observe in the species studied here. In horizontal sections, it is obvious that it projects into the central PN (Figure 8b), and it is therefore possible that it also sends some neurites to the MB. If these connections exist, they must be rather inconspicuous. We did not detect an equivalent of Bc4 in *A. bruennichi*, but this may be due to the lower selectivity of the Bodian stain in this species, compared to the other three species. However, anti-tubulin labeling also failed to detect Bc4, leading us to assume that it either belongs to a circuit that is not present in *A. bruennichi*, or that the neurites that comprise it are too thin to be detected with the methods used here. Babu and Barth (1984) described a protocerebro-median tract (PCMt) in *C. salei*, formed by the fusion of MCt, Ct, CLt, and VLt tracts before splitting up again into the protocerebral tracts LCt, MeCt, and VMt. We could not confirm the presence of this tract (Table 3). Instead, we were able to follow the course of each longitudinal tract into the PN, where they appear to taper but do not merge (Figure 9a,e,f). While we reported that LCt and MeCt both join the SLt near the esophagus, we could not find any connections of the VMt to the VNC (Figures 7 and 16). All longitudinal tracts from the VNC tightly adjoin as they pass the esophageal connective, and although this was not observed here, it is quite possible that neurites cross over into different tracts.

4.5 | Tracts in the VNC

Babu and Barth (1984) identified four commissures: DC, MDC, CC, and VC in *C. salei*. Babu and Barth (1989) also mention four commissures, but they are termed DC, MDC, MCC, and CC. It is unclear whether MCC constitutes a newly identified fifth commissure and VC was omitted, or whether CC from the earlier study was renamed MCC and VC from the earlier artcle was renamed CC. Later, Becherer and Schmid (1999) redrew the figure from Babu and Barth (1989) and added the VC as the fifth commissure without justifying this or indicating that they significantly altered the original drawing. In the four spider species investigated here, we found that Dc and MDc tightly adjoin and a separation is not possible with the methods used here. We also did not detect an MCc in the studied web-building hunters *A. bruennichi* and *P. tepidariorum* but were able to detect it in *P. amentata* and *M. muscosa*. It seems unlikely that the web-building hunters would lack this fifth commissure, and it is well possible that it is tightly adjoining one of the neighboring commissures (much like Dc and MDc).

Babu and Barth (1984, 1989) identified and described five "sensory longitudinal tracts (SLt)" in the cVNC of *C. salei*. They termed them "sensory" because they found that many sensory neurons from the legs terminate in the tracts. Because these sensory neurons project both into the posterior and the anterior direction, they concluded that the SLts must consist of both descending and ascending neurons (Babu & Barth, 1984; Figure 16). In the species studied here, we could not distinguish five different SLts, but only a single, large SLt occupying the most central part of the VNC (Figures 14a and 16). This could be partially due to the methods employed here, as we were unable to identify the termination sites of the sensory neurons, which might reveal a patterning not visible in Bodian stains and anti-tubulin immunolabeled material. However, the position, color and thickness of neurites that make up the SLt (Figures 11d and 14a) clearly show that it is identical to the SLts described in *C. salei* (Babu & Barth, 1984). We can therefore assume that the arrangement of afferent sensory neurons is similar to the one in *C. salei* in the four species described here.

While the cVNC is characterized by the six prominent longitudinal tracts, it also houses several neuropilar structures that receive direct sensory input (Babu & Barth, 1989). In addition to the LN, sensory neurons also project directly to the SLts, the LSAt, and even onto some of the longitudinal tracts (Babu & Barth, 1989; Gronenberg, 1990). A third termination site of sensory neurons within the cVNC is the BN, which receives input from hygro- and thermoreceptors and has so far only been found in *C. salei* (Anton & Tichy, 1994; Figure 16). We found a candidate structure in *P. amentata* and *M. muscosa* that very likely is the BN (Figure 10c). However, anterograde tracing of sensilla is required to explore this assumption. Such testing could also show whether the BN is truly absent or only less conspicuous in *A. bruennichi* and *P. tepidariorum*.

4.6 | Volumetric differences

Differences in sensory ecology often correlate with differences in the volume of CNS areas (Chittka & Niven, 2009). Larger volumes typically occur especially in sensory processing areas of the CNS and provide improved performance, such as a finer resolution or higher sensitivity of the sensory system (Chittka & Niven, 2009). We can thus expect the largest volume differences between web-building and cursorial hunting spiders in the CNS areas that process sensory information, whereas differences in CNS areas that consist mainly of non-synaptic areas, i.e. tracts should be less pronounced. Indeed, this is what we found in the four species studied here (Figure 15). The differences in the proportional volume of CNS areas clearly reflect differences in lifestyle: Neuropils that process mainly visual information are proportionally much larger in the cursorial hunting spiders, while the opposite is true for the LN that process mechanosensory information. We found very few differences in the cVNC and the PN, which both comprise many tracts but also comprise a number of neuropilar, sensory processing areas. It should be noted that the proportional volume of the neuropils associated with the principal eyes is the same in *P. amentata* and *A. bruennichi*, suggesting a similar importance of the visual information collected by these eyes. The volume differences observed in the OpN might be related to the fact that *A. bruennichi* and *P. tepidariorum* spin webs, a complicated task that involves specific movements and the precise use of various silk glands (Foelix, 2011; Kovoor, 1987). *Pardosa amentata* has the proportionally largest PdN, about twice that of *P. tepidariorum*, while the other two species have volumes in between. These species-specific differences possibly indicate behavioral differences in the use of the pedipalps, which would need to be explored in future studies. It is interesting that the ChN has a similar size in all species,

although it processes primary sensory information. Likely, the amount and quality of information gathered by the sensilla on the chelicerae is similar in all species. The similarity in the proportional volume of the AB supports the notion that it is not (in contrast to the MB) primarily a higher order visual neuropil but of overarching importance (see Functional Considerations section).

4.7 | Functional considerations

With the additional information on spider CNS anatomy and connectivity provided here, a refined picture emerges of the functional relationships of CNS areas and variation among different groups of spiders (Table 3; Figure 16). While the LN1-4, ChN, and PdN process sensory information from their respective appendages (Anton & Tichy, 1994; Babu & Barth, 1989; Gronenberg, 1989), they also house a "motor region" consisting of efferent neurites (Babu & Barth, 1989; Schmid & Becherer, 1999). More proximal neuropil regions such as the LSAt, SLt, BN, and to some extent the longitudinal tracts also receive direct sensory information and, in addition, are innervated by interneurons from various CNS regions, potentially serving as higher order integration centers within the VNC (Figure 16). Apart from being processed within the VNC, sensory information is also sent to various regions in the brain (Gronenberg, 1990) and likely processed in the PN and the AB. The present study shows that the arrangement of tracts and neuropil regions is similar in spider species that differ greatly in lifestyle (Table 3; Figure 16), and it is therefore reasonable to assume that these similarities also extend to functionality.

The brain receives direct sensory information from the eyes, and the visual pathways, particularly of the secondary eyes, vary greatly in spiders (Hanström, 1921; Long, 2021; Steinhoff et al., 2020; this study). These anatomical differences most likely result in different functionality. Cursorial hunting spiders detect motion with their secondary eyes (Schmid, 1998; Zurek & Nelson, 2012; Zurek et al., 2010), which provide input to the MB. At least one type of neuron originating at the MB innervates the motor region of the LN (Gronenberg, 1990), which suggests that the MB play a role in vision-guided motion control. Visual motion detection is thus likely to be much less well-developed or even absent in web-building spiders that do not possess MB such as *P. tepidariorum*. The evolution of three- dimensional webs, such as those built by *P. tepidariorum*, was likely largely driven by predator avoidance (Blackledge et al., 2002), which in turn might allow for smaller eyes and reduced visual processing in the brain.

While MB vary greatly among spider species (Long, 2021; Steinhoff et al., 2020; this study), the AB is very similar and always present, even in spiders that lack eyes (personal observation, unpublished). Furthermore, the relative size of the AB is similar in all species studied here and does not correlate with web-building (Weltzien & Barth, 1991). This observation, and the fact that the AB is well connected to both the VNC and the brain, suggests that it is not specifically dependent on a particular type of sensory input but plays a fundamental role in the integration of broad, multimodal sensory information and possibly motor control. To further investigate the functions of the CNS regions described here, electrophysiological recordings from single neurons in combination with dye backfills are required (cf. Gronenberg, 1990). For example, analysis of the central processing of olfactory information represents one promising avenue of future neurobiological research in spiders. The comparative morphological findings of this study provide the basis for physiological studies on the sensory ecology of spiders.

AUTHOR CONTRIBUTIONS

All authors had full access to all the data in the study and take responsibility for the integrity of the data and the accuracy of data analysis. Philip O. M. Steinhoff and Gabriele Uhl developed the concept and design. Philip O. M. Steinhoff acquired the data. Philip O. M. Steinhoff analyzed and interpreted the data. Philip O. M. Steinhoff wrote the manuscript. Gabriele Uhl and Steffen Harzsch contributed to the writing of the manuscript. Gabriele Uhl, Steffen Harzsch, and Philip O. M. Steinhoff obtained funding.

ACKNOWLEDGMENTS

We thank Nick Strausfeld and Gabriella Wolff for valuable tips on the Bodian-staining method. Ingrid Handt granted access to the greenhouses of the botanical garden, and Shou-Wang Lin helped with microCT reconstructions. We thank Heidi Land for discussions on the details of the histology. We thank Georg Brenneis and Jakob Krieger for critical discussions that helped to improve the manuscript. This study was financially supported by the German Research Foundation DFG UH 87/11-1 and DFG INST 292/119-1 FUGG, DFG INST 292/120-1 FUGG. Philip O. M. Steinhoff was supported by a Bogislaw Scholarship from the University of Greifswald during part of the project and a Laudier Histology Cooperation and Travel Grant.

Open access funding enabled and organized by Projekt DEAL.

CONFLICT OF INTEREST STATEMENT

The authors declare no conflicts of interest.

DATA AVAILABILITY STATEMENT

All serial Bodian-stained sections used to identify and reconstruct CNS structures, as well as three-dimensional (3D) PDFs of all reconstructed nervous systems are available from Morphobank using the URL: https://morphobank.org/permalink/?P4539 Image stacks are stored under "Media", the 3D PDFs as well as a list with all reconstructed CNS volumes are stored under "Documents."

ORCID

Philip O. M. Steinhoff https://orcid.org/0000-0003-1676-8105
Steffen Harzsch https://orcid.org/0000-0002-8645-3320
Gabriele Uhl https://orcid.org/0000-0001-8758-7913

REFERENCES

Anton, S., & Tichy, H. (1994). Hygro- and thermoreceptors in tip-pore sensilla of the tarsal organ of the spider *Cupiennius salei*: Innervation and central projection. *Cell and Tissue Research*, *278*, 399–407.

Babu, K. S. (1965). Anatomy of the central nervous system of arachnids. *Zoologische Jahrbücher. Abteilung für Anatomie und Ontogenie der Tiere*, *82*, 1–154.

Babu, K. S., & Barth, F. G. (1984). Neuroanatomy of the central nervous system of the wandering spider, *Cupiennius salei* (Arachnida, Araneida). *Zoomorphology*, *104*(6), 344–359. https://doi.org/10.1007/BF00312185

Babu, K. S., & Barth, F. G. (1989). Central nervous projections of mechanoreceptors in the spider *Cupiennius salei* Keys. *Cell and Tissue Research*, *258*(1), 69–82. https://doi.org/10.1007/BF00223146

Barth, F. G. (2002). *A spider's world: Senses and behavior*. Springer-Verlag.

Barth, F. G., Nakagawa, T., & Eguchi, E. (1993). Vision in the ctenid spider *Cupiennius salei*: Spectral range and absolute sensitivity. *Journal of Experimental Biology*, *79*, 63–79. https://doi.org/10.1242/jeb.181.1.63

Barth, F. G., & Seyfarth, E.-A. (1979). *Cupiennius salei* Keys. (Araneae) in the highlands of central Guatemala. *The Journal of Arachnology*, *7*(3), 255–263.

Bitsch, J., & Bitsch, C. (2007). The segmental organization of the head region in Chelicerata: A critical review of recent studies and hypotheses. *Acta Zoologica*, *88*(4), 317–335. https://doi.org/10.1111/j.1463-6395.2007.00284.x

Blackledge, T. A., Coddington, J. A., & Gillespie, R. G. (2002). Are three-dimensional spider webs defensive adaptations? Spider webs as predator defences. *Ecology Letters*, *6*(1), 13–18. https://doi.org/10.1046/j.1461-0248.2003.00384.x

Bodian, D. (1936). A new method for staining nerve fibers and nerve endings in mounted paraffin sections. *The Anatomical Record*, *65*(1), 89–97. https://doi.org/10.1002/ar.1090650110

Brenneis, G., Ungerer, P., & Scholtz, G. (2008). The chelifores of sea spiders (Arthropoda, Pycnogonida) are the appendages of the deutocerebral segment. *Evolution & Development*, *10*(6), 717–724. https://doi.org/10.1111/j.1525-142X.2008.00285.x

Chittka, L., & Niven, J. (2009). Are bigger brains better? *Current Biology*, *19*(21), R995–R1008. https://doi.org/10.1016/j.cub.2009.08.023

Couto, A., Wainwright, J. B., Morris, B. J., & Montgomery, S. H. (2020). Linking ecological specialisation to adaptations in butterfly brains and sensory systems. *Current Opinion in Insect Science*, *42*, 55–60. https://doi.org/10.1016/j.cois.2020.09.002

Damen, W. G. M., & Tautz, D. (1998). A Hox class 3 orthologue from the spider *Cupiennius salei* is expressed in a Hox-gene-like fashion. *Development Genes and Evolution*, *208*(10), 586–590. https://doi.org/10.1007/s004270050218

Doeffinger, C., Hartenstein, V., & Stollewerk, A. (2010). Compartmentalisation of the precheliceral neuroectoderm in the spider *Cupiennius salei*: Development of the arcuate body, the optic ganglia and the mushroom body. *The Journal of Comparative Neurology*, *518*(13), 2612–2632. https://doi.org/10.1002/cne.22355

Fenk, L. M., Hoinkes, T., & Schmid, A. (2010). Vision as a third sensory modality to elicit attack behavior in a nocturnal spider. *Journal of Comparative Physiology A*, *196*(12), 957–961. https://doi.org/10.1007/s00359-010-0575-8

Foelix, R. (2011). *Biology of spiders*. Oxford University Press.

Gregory, G. E. (1980). The Bodian Protargol technique. In N. J. Strausfeld, & T. A. Miller (Eds.), *Neuroanatomical techniques insect nervous system* (pp. 75–95). Springer-Verlag.

Gronenberg, W. (1989). Anatomical and physiological observations on the organization of mechanoreceptors and local interneurons in the central nervous system of the wandering spider *Cupiennius salei*. *Cell and Tissue Research*, *258*(1), 163–175. https://doi.org/10.1007/BF00223155

Gronenberg, W. (1990). The organization of plurisegmental mechanosensitive interneurons in the central nervous system of the wandering spider *Cupiennius salei*. *Cell and Tissue Research*, *260*, 49–61.

Hanström, B. (1921). Über die Histologie und vergleichende Anatomie der Sehganglien und Globuli der Araneen. *Kungliga Svenska Vetenskapsakademiens Handlingar*, *61*(12), 1–39.

Homann, H. (1950). Die Nebenaugen der Araneen. *Zoologische Jahrbücher. Abteilung für Anatomie und Ontogenie der Tiere*, *71*, 56–144.

Homann, H. (1952). Die Nebenaugen der Araneen. 2. Mitteilung. *Zoologische Jahrbücher. Abteilung für Anatomie und Ontogenie der Tiere*, *72*, 345–364.

Kovoor, J. (1987). Comparative structure and histochemistry of silk-producing organs in arachnids. In W. Nentwig (Ed.), *Ecophysiology of spiders* (pp. 160–186). Springer-Verlag.

Kovoor, J., Muñoz-Cuevas, A., & Ortega-Escobar, J. (2005). The visual system of *Lycosa tarentula* (Araneae, Lycosidae): Microscopic anatomy of the protocerebral optic centres. *Italian Journal of Zoology*, *72*(3), 205–216. https://doi.org/10.1080/11250000509356673

Land, M. F. (1972). Mechanisms of orientation and pattern recognition by jumping spiders (Salticidae). In R. Wehner (Ed.), *Information processing in the visual systems of anthropods* (pp. 231–247). Springer-Verlag. https://doi.org/10.1007/978-3-642-65477-0_34

Land, M. F. (1985). The morphology and optics of spider eyes. In F. G. Barth (Ed.), *Neurobiology of arachnids* (pp. 53–76). Springer-Verlag. https://doi.org/10.1007/978-3-642-70348-5_4

Lehmann, T., Melzer, R., Hörnig, M. K., Michalik, P., Sombke, A., & Harzsch, S. (2016). Arachnida (excluding Scorpiones). In A. Schmidt-Rhaesa, S. Harzsch, & G. Purschke (Eds.), *Structure and evolution of invertebrate nervous systems*. Oxford University Press. https://doi.org/10.1093/acprof:oso/9780199682201.001.0001

Loesel, R., Seyfarth, E.-A., Bräunig, P., & Agricola, H.-J. (2011). Neuroarchitecture of the arcuate body in the brain of the spider *Cupiennius salei* (Araneae, Chelicerata) revealed by allatostatin-, proctolin-, and CCAP-immunocytochemistry and its evolutionary implications. *Arthropod Structure & Development*, *40*(3), 210–220. https://doi.org/10.1016/j.asd.2011.01.002

Long, S. M. (2021). Variations on a theme: Morphological variation in the secondary eye visual pathway across the order of Araneae. *The Journal of Comparative Neurology*, *529*(2), 259–280. https://doi.org/10.1002/cne.24945

Louail, M., Gilissen, E., Prat, S., Garcia, C., & Bouret, S. (2019). Refining the ecological brain: Strong relation between the ventromedial prefrontal cortex and feeding ecology in five primate species. *Cortex*, *118*, 262–274. https://doi.org/10.1016/j.cortex.2019.03.019

Mittmann, B., & Scholtz, G. (2003). Development of the nervous system in the "head" of *Limulus polyphemus* (Chelicerata: Xiphosura): Morphological evidence for a correspondence between the segments of the chelicerae and of the (first) antennae of Mandibulata. *Development Genes and Evolution*, *213*(1), 9–17. https://doi.org/10.1007/s00427-002-0285-5

Montgomery, S. H., Rossi, M., McMillan, W. O., & Merrill, R. M. (2021). Neural divergence and hybrid disruption between ecologically isolated *Heliconius* butterflies. *Proceedings of the National Academy of Sciences*, *118*(6), e2015102118. https://doi.org/10.1073/pnas.2015102118

Morehouse, N. I., Buschbeck, E. K., Zurek, D. B., Steck, M., & Porter, M. L. (2017). Molecular evolution of spider vision: New opportunities, familiar players. *Biological Bulletin*, *233*(1), 21–38. https://doi.org/10.1086/693977

Ott, S. R. (2008). Confocal microscopy in large insect brains: Zinc–formaldehyde fixation improves synapsin immunostaining and preservation of morphology in whole-mounts. *Journal of Neuroscience Methods*, *172*(2), 220–230. https://doi.org/10.1016/j.jneumeth.2008.04.031

Pan, X., Bourland, W. A., & Song, W. (2013). Protargol synthesis: An in-house protocol. *Journal of Eukaryotic Microbiology*, *60*(6), 609–614. https://doi.org/10.1111/jeu.12067

Park, Y.-K., Kim, H.-J., Kim, H., & Moon, M.-J. (2013). Fine structure of the CNS ganglia in the geometric spider *Nephila clavata* (Araneae: Nephilidae). *Entomological Research*, *43*(6), 330–343. https://doi.org/10.1111/1748-5967.12039

Richter, S., Loesel, R., Purschke, G., Schmidt-Rhaesa, A., Scholtz, G., Stach, T., Vogt, L., Wanninger, A., Brenneis, G., Döring, C., Faller, S., Fritsch, M.,

Grobe, P., Heuer, C. M., Kaul, S., Møller, O. S., Müller, C. H., Rieger, V., Rothe, B. H., … Harzsch, S. (2010). Invertebrate neurophylogeny: suggested terms and definitions for a neuroanatomical glossary. *Frontiers in Zoology*, *7*(1), 29. https://doi.org/10.1186/1742-9994-7-29

Rivera Quiroz, F. A., & Miller, J. (2022). Micro-CT visualization of the CNS: Performance of different contrast-enhancing techniques for documenting the spider brain. *The Journal of Comparative Neurology*, *530*(14), 2474–2485. https://doi.org/10.1002/cne.25343

Schmid, A. (1998). Different functions of different eye types in the spider *Cupiennius salei*. *The Journal of Experimental Biology*, *201*, 221–225.

Schmid, A., & Becherer, C. (1999). Distribution of histamine in the CNS of different spiders. *Microscopy Research and Technique*, *44*(2-3), 81–93. https://doi.org/10.1002/(SICI)1097-0029(19990115/01)44:2/3⟨81::AID-JEMT3⟩3.0.CO;2-O

Schmid, A., & Duncker, M. (1993). Histamine immunoreactivity in the central nervous system of the spider *Cupiennius salei*. *Cell and Tissue Research*, *273*, 533–545.

Scholtz, G. (2016). Perspective—Heads and brains in arthropods: 40 years after the endless dispute. In A. Schmidt-Rhaesa, S. Harzsch, & G. Purschke (Eds.), *Structure and evolution of invertebrate nervous systems* (pp. 402–410). Oxford University Press.

Scholtz, G., & Edgecombe, G. D. (2006). The evolution of arthropod heads: Reconciling morphological, developmental and palaeontological evidence. *Development Genes and Evolution*, *216*(7-8), 395–415. https://doi.org/10.1007/s00427-006-0085-4

Schulze, E., & Graupner, H. (1960). *Anleitung zum mikroskopisch-technischen Arbeiten in Biologie und Medizin*. Akademische Verlagsgesellschaft.

Sombke, A., Lipke, E., Michalik, P., Uhl, G., & Harzsch, S. (2015). Potential and limitations of X-Ray micro-computed tomography in arthropod neuroanatomy: A methodological and comparative survey: Micro-CT in arthropod neuroanatomy. *The Journal of Comparative Neurology*, *523*(8), 1281–1295. https://doi.org/10.1002/cne.23741

Steinhoff, P. O. M., Sombke, A., Liedtke, J., Schneider, J. M., Harzsch, S., & Uhl, G. (2017). The synganglion of the jumping spider *Marpissa muscosa* (Arachnida: Salticidae): Insights from histology, immunohistochemistry and microCT analysis. *Arthropod Structure and Development*, *46*(2), 156–170. https://doi.org/10.1016/j.asd.2016.11.003

Steinhoff, P. O. M., Uhl, G., Harzsch, S., & Sombke, A. (2020). Visual pathways in the brain of the jumping spider *Marpissa muscosa*. *The Journal of Comparative Neurology*, *528*(11), 1883–1902. https://doi.org/10.1002/cne.24861

Strausfeld, N. J. (2012). *Arthropod brains: Evolution, functional elegance, and historical significance*. Harvard University Press.

Strausfeld, N. J., & Barth, F. G. (1993). Two visual systems in one brain: Neuropils serving the secondary eyes of the spider *Cupiennius salei*. *The Journal of Comparative Neurology*, *328*(1), 43–62. https://doi.org/10.1002/cne.903280104

Strausfeld, N. J., Sinakevitch, I., Brown, S. M., & Farris, S. M. (2009). Ground plan of the insect mushroom body: Functional and evolutionary implications. *The Journal of Comparative Neurology*, *513*(3), 265–291. https://doi.org/10.1002/cne.21948

Strausfeld, N. J., Weltzien, P., & Barth, F. G. (1993). Two visual systems in one brain: Neuropils serving the principal eyes of the spider *Cupiennius salei*. *The Journal of Comparative Neurology*, *328*(1), 63–75. https://doi.org/10.1002/cne.903280105

Wegerhoff, R., & Breidbach, O. (1995). Comparative aspects of the chelicerate nervous systems. In O. Breidbach & W. Kutsch (Eds.), *The nervous systems of invertebrates: An evolutionary and comparative approach* (Vol. 72, pp. 159–179). Birkhäuser Basel. https://doi.org/10.1007/978-3-0348-9219-3_9

Weltzien, P., & Barth, F. G. (1991). Volumetric measurements do not demonstrate that the spider brain "central body" has a special role in web building. *Journal of Morphology*, *208*(1), 91–98. https://doi.org/10.1002/jmor.1052080104

Weygoldt, P. (1975). Untersuchungen zur Embryologie und Morphologie der Geißelspinne *Tarantula marginemaculata* C. L. Koch (Arachnida, Amblypygi, Tarantulidae). *Zoomorphologie*, *82*, 137–199.

Weygoldt, P. (1985). Ontogeny of the arachnid central nervous system. In F. G. Barth (Ed.), *Neurobiology of arachnids* (pp. 20–37). Springer-Verlag.

Wolff, G. H., & Strausfeld, N. J. (2015). Genealogical correspondence of mushroom bodies across invertebrate phyla. *Current Biology*, *25*(1), 38–44. https://doi.org/10.1016/j.cub.2014.10.049

Yamashita, S., & Tateda, H. (1976). Spectral sensitivities of jumping spider eyes. *Journal of Comparative Physiology A*, *105*(1), 29–41. https://doi.org/10.1007/BF01380051

Yamashita, S., & Tateda, H. (1978). Spectral sensitivities of the anterior median eyes of the orb web spiders, *Argiope bruennichii* and *A. amoena*. *Journal of Experimental Biology*, *74*(1), 47–57.

Zurek, D. B., & Nelson, X. J. (2012). Hyperacute motion detection by the lateral eyes of jumping spiders. *Vision Research*, *66*, 26–30. https://doi.org/10.1016/j.visres.2012.06.011

Zurek, D. B., Taylor, A. J., Evans, C. S., & Nelson, X. J. (2010). The role of the anterior lateral eyes in the vision-based behaviour of jumping spiders. *Journal of Experimental Biology*, *213*(14), 2372–2378. https://doi.org/10.1242/jeb.042382

How to cite this article: Steinhoff, P. O. M., Harzsch, S., & Uhl, G. (2024). Comparative neuroanatomy of the central nervous system in web-building and cursorial hunting spiders. *Journal of Comparative Neurology*, *532*, e25554. https://doi.org/10.1002/cne.25554